Estimates of the Annual Net Carbon and Water Exchange of Forests: The EUROFLUX Methodology

M. AUBINET, A. GRELLE, A. IBROM, Ü. RANNIK, J. MONCRIEFF, T. FOKEN, A.S. KOWALSKI, P.H. MARTIN, P. BERBIGIER, CH. BERNHOFER, R. CLEMENT, J. ELBERS, A. GRANIER, T. GRÜNWALD, K. MORGENSTERN, K. PILEGAARD, C. REBMANN, W. SNIJDERS, R. VALENTINI AND T. VESALA

ADVANCES IN ECOLOGICAL RESEARCH VOL. 30
ISBN 0-12-013930-8

I. INTRODUCTION

The dramatic increase in the concentration of carbon dioxide (CO_2) in the atmosphere since the industrial revolution of the mid-nineteenth century constitutes a chemical change of global proportions. This increase in a radiatively active trace gas is the most obvious consequence of industrialization and is well documented (Houghton *et al.*, 1996). Fossil fuel combustion and deforestation explain most of this long-term increase in atmospheric CO_2 concentration, yet the pathways and processes that determine the dynamics of the global carbon cycle remain largely unknown. For example, the ultimate fate of half of the anthropogenically released CO_2 is uncertain in that this 'missing sink' may be in the terrestrial biosphere, the soil or the ocean, or some combination of all three (Schimel, 1995; Houghton *et al.*, 1998). Such incomplete knowledge as well as uncertainties in the fluxes between parts of the system adds to the uncertainty in estimations of the present state of the global carbon cycle. Inadequate specification of the system also limits predictions about its response to natural and anthropogenic perturbations. Fortunately, long-term studies of gaseous exchanges between the biosphere and the atmosphere can help by filling knowledge gaps and building a stronger predictive capability. It is against this background that the EUROFLUX project was established: this chapter describes the methodology that is common to all partners within the programme.

By definition, long-term studies of the exchange between the biosphere and the atmosphere require direct and continuous measurement of water vapour and CO_2 transfer. Micrometeorological methods such as eddy covariance offer a means to monitor directly the exchange of trace gases between the biosphere and the atmosphere (Moncrieff *et al.* (1997b). In this technique, eddies are sampled for their vertical velocity and concentration of scalar of interest (e.g. H_2O or CO_2). Averaging these recorded fluctuations in gas concentrations over a period of about 30 min yields the net amount of material being transported in the vertical above the surface. Swinbank (1951) proposed and tested the fundamental concepts of eddy covariance but the difficulties associated with instrumentation and data collection were not overcome until some three decades later. A number of systems have now been described in the literature (Lloyd *et al.*, 1984; Businger, 1986; McMillen,1988; Grelle and Lindroth, 1996; Moncrieff *et al.*, 1997a). This method was used to carry out flux measurement campaigns on increasing time-scales. The first campaigns were limited to 1 or 2 weeks. Reports of such experiments were presented, notably,

by Desjardins (1985) on maize, by Verma *et al.* (1986) on tallgrass prairie, by Valentini *et al.* (1991) on Mediterranean macchia, and by Verma *et al.* (1989), Baldocchi and Meyers (1991) and Hollinger *et al.* (1994) on forests. Campaigns extended on a full growing season were presented later by Grace *et al.* (1996) on Amazonian forest, by Valentini *et al.* (1996) on a beech forest, and by Baldocchi *et al.* (1997) and Jarvis *et al.* (1997) on different types of boreal forests.

The first annual time-scale CO_2 flux measurement campaigns above forests using the eddy covariance technique were organized in the early 1990s in North America (Wofsy *et al.*, 1993; Black *et al.*, 1996; Goulden *et al.*, 1996a,b; Greco and Baldocchi, 1996) and Europe (Lindroth *et al.*, 1998). In addition, annual time-scale CO_2 flux measurements were performed by teams using other micrometeorological techniques such as the Bowen ratio or aerodynamic techniques (Vermetten *et al.*, 1994; Saigusa *et al.*, 1998). These early results extended our knowledge of the different ecosystem behaviours, but each was limited to a particular ecosystem. However, no attempt at a systematic study across related biomes and across climate scales was made. The conclusions of an International Geosphere-Biosphere Program (IGBP)-sponsored workshop for global change scientists held at La Thuile, Italy, in 1996 highlighted the need for regional networks of flux measurement stations sited across a broad spectrum of ecosystems and climatic environments (Baldocchi *et al.*, 1996).

The EUROFLUX project, sponsored by the Fourth Framework Programme of the European Commission, arose shortly after this workshop to meet this need. A fundamental premise of the EUROFLUX project was to make continuous and long-term (at least three complete annual cycles) of carbon and water exchange between European forests and the atmosphere. EUROFLUX also sought to provide information about the role of the terrestrial biosphere in the climate system. This was attempted for forests of different types and under different climate regimes. The outputs from the project will include not only a better understanding of the functioning of forests but also their role in climate change. Results from EUROFLUX should contribute to mesoscale or general circulation models of the atmosphere by improving surface parameterizations and aggregation schemes in order to scale up to global scale. The important issue of how forest management practices can alter ecosystem water and carbon balances (and the role of forests in the sequestration of carbon) is a further output of the project. The Protocol on Climate negotiated during the third session of the United Nation (UN) Framework Convention on Climate Change (FCCC), signed in Kyoto on 11 December 1997, strengthened the interest in continental-scale measurement networks and the kind of studies described above. The Kyoto Protocol also revealed the immediate policy relevance of EUROFLUX, which thus became much more than a well-orchestrated academic exercise.

The EUROFLUX network includes 14 measuring stations and encompasses a large range of latitudes (from 41.45N to 64.14N), climates (Mediterranean, temperate, arctic) and species (*Quercus, Fagus, Pseudotsuga, Pinus, Picea*). Table 1 provides information on each of the 14 sites. Scaling up measurements from the local scale to the European continent (Martin *et al.*, 1998) and site intercomparisons constitute a central objective of EUROFLUX. This imposes on the partners within the programme the adoption of a series of common methodologies for the measurement of fluxes and for the correction and treatment of data. It is these methodologies, which are used in the EUROFLUX network, that are presented here.

In the first part of the chapter (III to VII), the measurement system and the procedure followed for the computation of the fluxes is described. In the second part (VIII to XI), the procedure of flux summation, including data gap-filling strategy, night flux corrections and error estimation is presented.

II. THEORY

The conservation equation of a scalar is:

$$\frac{\partial \rho_s}{\partial t} + u\frac{\partial \rho_s}{\partial x} + v\frac{\partial \rho_s}{\partial y} + w\frac{\partial \rho_s}{\partial z} = S + D \tag{1}$$

where ρ_s is the scalar density, u, v and w are the wind velocity components, respectively, in the direction of the mean wind (x), the lateral wind (y) and normal to the surface (z). S is the source/sink term and D is molecular diffusion. The lateral gradients and the molecular diffusion will be neglected afterwards. After application of the Reynolds decomposition where: $u = \bar{u} + u'$, $v = \bar{v} + v'$, $w = \bar{w} + w'$, $\rho_s = \bar{\rho}_s + \rho_s'$, where the overbars characterize time averages and the primes indicate fluctuations around the average, integration along z and assumption of no horizontal eddy flux divergence, equation (1) becomes:

$$\int_0^{h_m} S dz = \overline{w'\rho_s'} + \int_0^{h_m} \frac{\partial \overline{\rho_s}}{\partial_t} dz + \int_0^{h_m} \bar{u}\frac{\partial \overline{\rho_s}}{\partial x} dz + \int_0^{h_m} \bar{w}\frac{\partial \overline{\rho_s}}{\partial z} dz \tag{2}$$

I II III IV V

Term I represents the scalar source/sink term which corresponds to the net ecosystem exchange (N_e) when the scalar is CO_2, and to ecosystem evapotranspiration (E) when the scalar is water vapour. Term II represents the eddy flux at height h_m (the flux measured by eddy covariance systems). It is noted as F_c for carbon dioxide and F_w for water vapour. Under conditions of atmospheric stationarity and horizontal homogeneity, all the other terms on the

Table 1
Site characteristics

Participant	Site	Geographical co-ordinates	Dominant tree species	Age (years)	Canopy height (m)	Mean tree diameter (cm)	Tree density (ha^{-1})	Leaf Area Index ($m^2\ m^{-2}$)	Soil type
IT1	Collelongo	41° 52′ N, 13° 38′ E	*Fagus sylvatica*	100	22	18.1	885	4.5	Calcareous, brown earth (inceptisol)
IT2	Castel Porziano	41° 45′N, 12° 22′ E	*Quercus ilex*	50	12.5	16	1500	3.5	Sandy
FR1	Hesse	48° 40′ N, 7° 05′ E	*Fagus sylvatica*	25–30	13	10	4000	5.5	Luvisol to stagnic luvisol
FR2	Les Landes	44° 42′ N, 0° 46′ W	*Pinus pinaster*	36	18	26	500	2.5–3.5	Sandy podzol
DK1	Lille Boegeskov	55° 29″ 13′ N, 11° 38″ 45′ E	*Fagus sylvatica*	80	25	28	430	4.75	Cambisol
SW1	Norunda	60° 05′ N, 17° 28′ E	*Picea abies*, *Pinus sylvestris*	70–120	24	21	678	4–5	Deep sandy till
SW2	Flakkalinden	64° 07′ N, 19° 27′ E	*Picea abies*	35	8	8.5	2127	2.8	Shallow till
GE1	Bayreuth	50° 09′ N, 11° 52′ E	*Picea abies*	43	19	23	1000	6.7 ± 1.5	Brown earth (acidic cambisol)
NL1	Loobos	52° 10′ N, 5° 44′ E	*Pinus sylvestris*	97	15.1	25.4	362	3	Podzollic
UK1	Griffin	56° 37′ N, 3° 48′ W	*Picea sitchensis*	15	6	7	2500	About 8	Stony podsolized brown earth
GE2	Tharandt	50° 58′ N, 13° 38′ E	*Picea abies*	106	28	27	652	5	Brown earth
BE1	Vielsalm	50° 18′ N, 6° 00′ E	*Fagus sylvatica*, *Pseudotsuga menziesii*	60–90	27–35	34	230	5–5.3	Dystric cambisol
BE2	Braaschaat	51° 18′ N, 4° 31′ E	*Pinus sylvestris*, *Quercus robur*	67	22	26.8	542	3	Moderately wet sandy soil
FI1	Hyytiälä	61° 51′ N, 24° 17′ E	*Pinus sylvestris*	32	12	13	2500	3	Till

More information about the sites may be found at http://www.unitus.it/eflux/euro.html.

right-hand side of equation (2) decay and the measurement by eddy covariance is equivalent to the source/sink term. However, in forest systems (and others), these conditions are not always met and this approximation cannot always be made.

Term III represents the storage of the scalar below the measurement height. Storage of carbon dioxide, S_c, is typically small during the day and on windy nights. However, significant positive values may be observed during poor mixing conditions at night when the CO_2 produced by the ecosystem respiration is accumulating in the ecosystem. On the other hand, a negative peak of S_c is often observed in the morning when the CO_2 accumulated at night is flushed out of the ecosystem or absorbed by ecosystem assimilation (Grace *et al.*, 1996; Goulden *et al.*, 1996a). The daily mean of this term is zero, so ignoring it over the long term is acceptable. However, in the short term, it may be a significant measure of ecosystem response and should be taken into account. The storage of water vapour (S_w) is small at night, the ecosystem transpiration rate being low during this period.

Terms IV and V represent the fluxes by horizontal and vertical advection (V_c and V_w for CO_2 and water vapour respectively). Term IV is significant when horizontal gradients of scalar exist, i.e. in heterogeneous terrain or at night over sloping terrain, when the CO_2 produced by the ecosystem respiration is removed by drainage. The vertical velocity (w) and, consequently, the vertical advection (term V) were found typically to be zero over low crops. However, there is no such evidence above tall vegetation like forest canopies, and Lee (1998) and Baldocchi *et al.* (unpublished) have shown that this mechanism is not negligible and could even be more important than turbulent transport during calm nights. The advection terms are not measurable with available technology. These terms are probably responsible for the mismatch observed at night between N_e and $F_c + S_c$, as shown in section X below, and a procedure to correct these fluxes empirically is described.

Finally, using the notations introduced previously, equation (2) becomes:

$$N_e = F_c + S_c + V_c \tag{3}$$

F or CO_2 and:

$$E = F_w + S_w + V_w \tag{4}$$

for water vapour.

In the rest of this paper, we will first describe the measurement system (sections III and IV) and the procedures for computation, correction and data-quality analysis (section V) of the eddy fluxes F_c and F_w. The spatial representativeness of the fluxes is analysed in section VII. The procedure followed to obtain annual carbon sequestration is described in section VIII.

It also involves the data gap-filling strategy (section IX), the correction for night flux underestimation (section X) and the estimation of uncertainties (section XI).

III. THE EDDY COVARIANCE SYSTEM

A number of European laboratories collaborated in the early 1990s to produce a common design for an eddy covariance system for the HAPEX-Sahel project (Moncrieff *et al.*, 1997a), and this system formed the basis for that used in EUROFLUX. Other groups in Europe have independently arrived at very similar systems (Grelle and Lindroth, 1996). In essence, the flux systems comprise a three-axis sonic anemometer (Solent 1012R2; Gill Instruments, Lymington, UK), a closed-path infrafred gas analyser (LI-COR 6262; LI-COR, Lincoln, New England, USA) and a suite of analysis software for real-time and post-processing analysis. Gas samples are taken next to the sonic path and ducted down a sample tube to the infrared gas analyser (IRGA).

A. Sonic Anemometer

The sonic anemometer produces the values of the three wind components and the speed of sound at a rate of 20.8 times per second. A set of sound transit times can be obtained 56 times per second. In addition, it has a built-in five-channel analogue to digital (A/D) converter with an input range of 0–5 V and a resolution of 11 bits; this permits simultaneous measurement of analogue sensors and their digitization and integration with the turbulence signals. The analogue channels are sampled at a rate of 10 Hz. In the EUROFLUX system, the analogue channels are used for water vapour and CO_2 concentration output from the IRGA. Additional signals, such as air temperature, air flow through the analyser and analyser temperature, can also be accommodated in this way. Data from the sonic anemometer can be collected as either analogue or digital signals.

To avoid the need to turn the sensing volume of the anemometer into the mean wind direction, the omnidirectional probe head was chosen. The supporting rod and the probe head itself are quite slender and produce relatively little flow distortion (< 5% effect on scalar fluxes; Grelle and Lindroth, 1994). However, a wind tunnel calibration is recommended and at present is applied by only two groups (SW1 and 2, DK1). Before the EUROFLUX project, a sonic anemometer of the same type had been tested under Arctic conditions within the framework of ARKTIS-93 (Peters *et al.*, 1993; Grelle *et al.*, 1994) and proved to work reliably even at temperatures as low as −42°C.

Built-in memory on the circuit board enables the anemometer to store a maximum of 170 s worth of data, depending on the number of analogue inputs sampled. Some of the software in use within EUROFLUX uses the sonic in

'prompted mode' (i.e. data are transferred only by request). In this way, 'quasi on-line' processing of data can easily be carried out in the breaks between transmissions. Other software in use accepts the data stream in real time as it is sent out by the sonic ('unprompted' mode).

In some of the eddy covariance systems (SW1 and 2), the sonic probe head is mounted on a two-axis inclination sensor and/or an adjustable boom to correct for sensor misalignment (Grelle and Lindroth, 1996). In high wind speeds, vibrations of the boom that supports the sonic may introduce a significant bias in flux measurements, but making the boom asymmetrical may reduce these vibrations.

B. Temperature Fluctuation Measurements

Generally, measurement of air temperature fluctuations is done by means of the speed-of-sound output of the sonic anemometer. At wind speeds above about 8–10 m s^{-1}, however, speed-of-sound data become noisier because of mechanical deformation of the probe head (Figure 1). Determination of the sensible heat flux from the sonic measurements is impossible in these cases (Grelle and Lindroth, 1996). Thus, additional fast thermometers are applied at sites with frequent high wind speeds (SW1 and 2). Particularly at high wind speeds and over forest canopies, even relatively robust sensors possess a sufficiently fast frequency response to measure temperature fluctuations without considerable loss; for example, the use of platinum resistance wires was described by Grelle and Lindroth (1996).

C. Infrared Gas Analyser

The concentrations of water vapour and CO_2 are measured by a LI 6262 infrared gas analyser (IRGA). The IRGA is a differential analyser which compares the absorption of infrared energy by water vapour and CO_2 in two different chambers within the optical bench. Use of this instrument has been described in detail by Moncrieff *et al.* (1997a). In EUROFLUX, the analyser is used in absolute mode, i.e. the reference chamber is filled with a gas scrubbed of water and CO_2. For this purpose, two methods may be used: the manufacturer suggests a closed pump-driven air circuit through the reference cell with desiccant and CO_2-absorbing chemicals. Four teams (IT1 and 2, FR1, BE2) use this configuration (Figure 2a). However, it often results in a zero drift of the signals, which is apparently caused by the release of CO_2 by soda lime or ascarite when the reference air becomes too dry, and in some cases by leakage in the reference line. Leakages occur, for example, when the O-ring seals of the scrubber tubes are damaged by the influence of the chemicals. On the other hand, an open reference air stream is not practical for unattended long-term measurements, as the chemicals would need to be changed too often. The

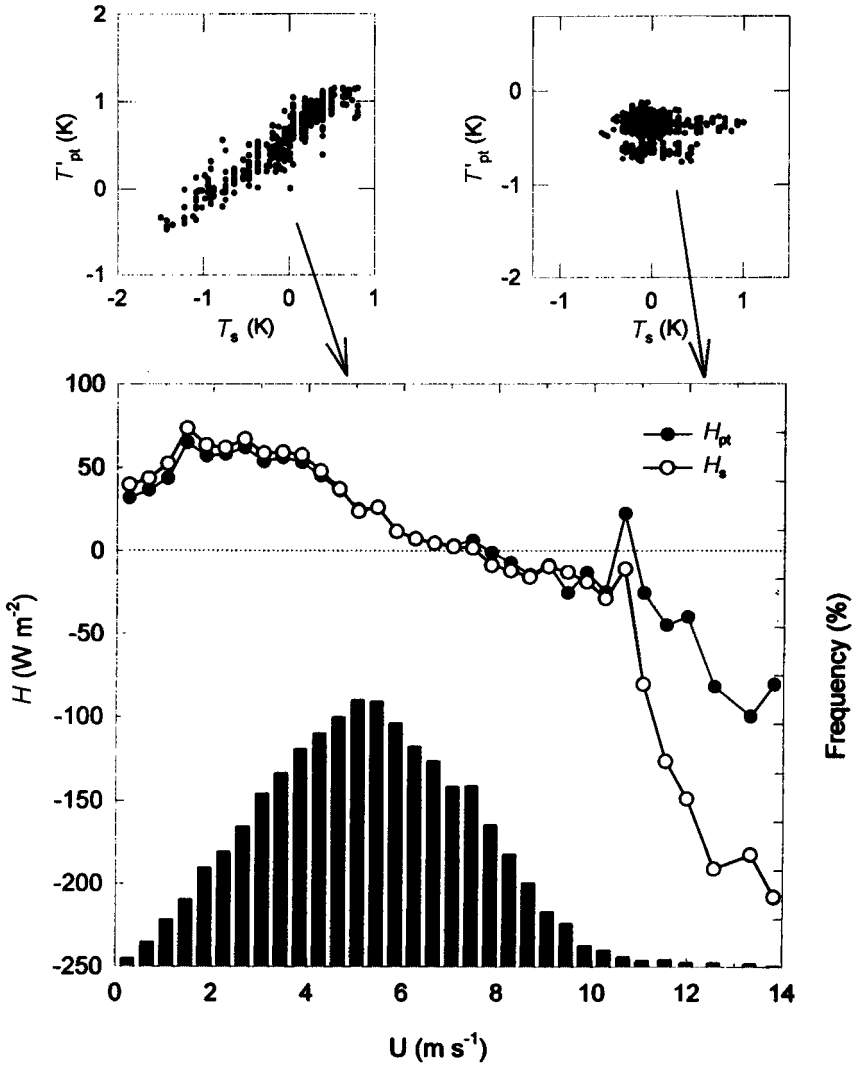

Fig. 1. Sensible heat flux by sonic temperature (H_s) and platinum wire thermometer (H_{pt}), classified by wind velocity. *Upper graphs*: Time series of temperature fluctuations, sonic temperature (T_{son}) versus platinum wire temperature (T_{pt}) at wind speeds of 4.4 and 12.2 m s^{-1}.

second method, which overcomes these problems, consists of flushing the reference chamber with nitrogen gas from a cylinder, maintaining a flow rate of about 20 ml min^{-1}. Ten teams use this configuration (FR2, DK1, UK1, SW1 and 2, NL1, GE1 and 2, BE1, F11) (Figure 2b). In systems that have different

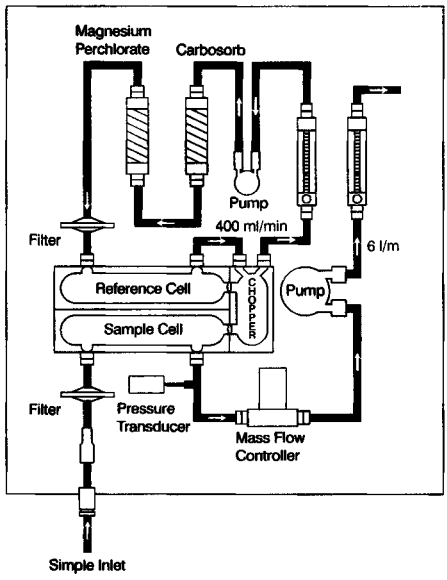

(a)

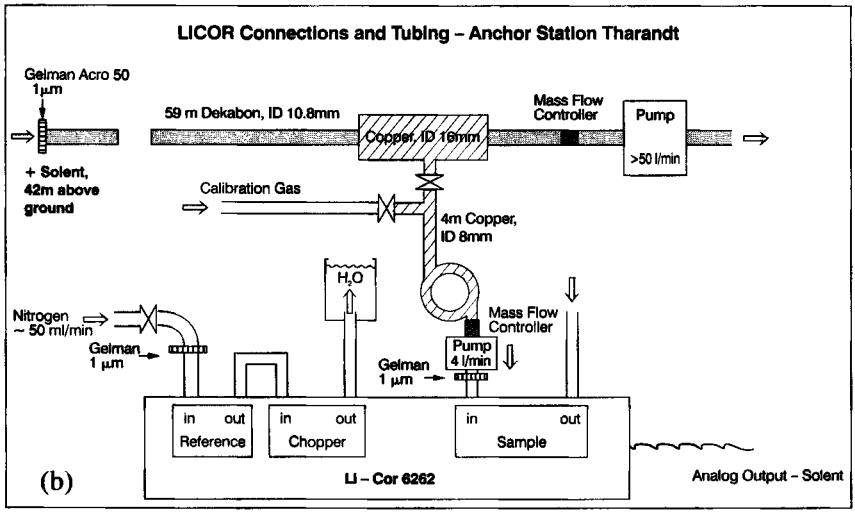

(b)

Fig. 2. Two typical flow configurations used in EUROFLUX. (a) System with through flow in the sample circuit and chemicals in the reference circuit (Moncrieff *et al.*, 1997a). (b) System with secondary flow in the sample circuit and nitrogen in the reference.

analysers at several levels on a tower, and when N_2 from one common source has to pass to different gas analysers, the chopper chambers of the gas analysers cannot be flushed by the common N_2 path because these chambers usually leak. In these cases, scrubber chemicals are used (SW1 and 2, GE1).

Calibration of the IRGA is carried out according to the preferences of the teams: some perform it automatically every day while others perform it manually at a lesser frequency (fortnightly). A lower calibration frequency may affect the mean CO_2 concentration measurement, as the LI-COR 6262 is subject to significant zero drift. However, as the slope drift is very low, the impact of the calibration frequency on the fluxes is limited.

The signals for water vapour and CO_2 concentration can be output in a variety of units from the IRGA, either as analogue voltage signals, analogue current signals, or as ASCII for serial communication. However, if a fast response is desired, the raw voltage signals for the CO_2 and water vapour mixing ratio should be used. With this configuration, the 95% time constant of the analyser is 0.1 s (LI-COR, 1991). Additionally, the internal analyser temperature can be obtained as an analogue signal.

D. Air Transport System

A variety of different airflow configurations is used by teams within the project. The technical specifications are given for each site in Table 2. The choice of flow configuration is determined according to a number of criteria:

(1) To minimize frequency loss (i.e. by maintaining flow with high Reynolds number (*Re*) in the inlet tube (Leuning and Moncrieff, 1990).
(2) To avoid condensation within tubes and analyser.
(3) To avoid pressure fluctuations and air contamination caused by the pump.
(4) To comply with the IRGA's range of operational parameters (e.g. pressure, chamber temperature).
(5) To stabilize and monitor the air flow.
(6) To keep the analyser chamber clean.

Most commonly, the analyser is placed on the tower, some metres away from the sonic. Some groups use long sample tubes with the analyser on the ground surface as this permits easy access to service the gas analyser (DK1, GE2).

To minimize frequency losses, turbulent airflow through the tube is sometimes chosen (GE2, SW1 and 2) (Moore, 1986), but this usually requires powerful pumps with a high power consumption. Laminar flow in the tube is maintained by less powerful pumps and the extra loss in frequency response can be accounted for adequately (Moncrieff *et al.*, 1997a). The data in Table 2 show that the EUROFLUX systems operate between *Re* 1800 and 6550 (where *Re* of about 2030 is generally considered as the cut-off for transition to turbulent flow) within the types of sample tube used here. However, several

Table 2
Technical specifications of the sites

Site	Pump type	Circuit	Q (l min^{-1})	Filters	L_t (m)	r_t (10^{-3} m)	L_s (m)	τ_{lr} (real) (s)	τ_{lc} (comp.) (s)	$F_{co\text{-}ss}$ (Hz)	a_{ss} (m^{-1})	*Re*
IT1	D	TS	12	2A	9.0	2.0	0.35	2.1	0.56	19.14	0.31	4245
IT2	D	TS	10.5	2A	3.0	2.0			0.22	26.07		3712
FR1	R	TS	6.0	A + S	30.0	2.0	0.2	3.9–4.1	3.8	2.48	0.54	2122
FR2	R	TS	8.0	A + S	3.0	2.0	0.2	1.9–2.2	0.28	15.30	0.54	2828
DK1	P	M	20.0		48.0	4.0	0.6	7.5–9.5	7.24	2.10	0.18	3535
SW1	2D	TB	9.9	2A	7.2	2.0	0.1	1.3–1.3	0.55	15.08	1.07	3503
SW2	2D	TB	11.6	2A	6.5	2.0	0.1	1.05	0.42	21.21	1.07	4105
GE1	R	TS	6.0	2A	7.0	3.15	0.2	2.5	0.55	12.9	0.54	2660
NL1	D	M	7.4		7.0	2.0			0.71	8.47		2616
UK1	D	TS	6.0	2A	18.0	3.2	0.15	6–6.5	5.2	0.53	0.71	1885
GE2	LD	M	50.0	2A	59.0	5.4	0.2	10–11.5	6.48	3.46	0.54	6546
BE1	D	TS	6.0	A + S	8.0	2.0	0.2	2.6–3.1	1.01	4.81	0.54	2122
BE2	R	TS	5.5	2A	3.0	2.2	0.48	1.5–2.0	0.48	2.37	0.22	1796
FI1	D	TS	6.3	1A	7.0	2.0	0.15	1.5–1.7	0.84	5.82	0.71	2227

Q, flow rate in tube; L_t tube length; r_t, tube radius; L_s, separation distance between the sonic anemometer (centre of the measurement volume) and the inlet tube; τ_l, time lag (r, measured; c, computed); $F_{co\text{-}ss}$, cut-off frequency characterizing the sensor separation effect; a_{ss}, slope of the relation between $F_{co\text{-}ss}$ and the mean wind speed (equation (27)). *Re*, Reynolds number; D, diaphragm; R, rotative; P, piston; 2D, double diaphragm; LD, linear diaphragm; TS, sucked through the analyser; TB, blown through the analyser; M, two pumps; 2A, 2 Acro 50 1 μm; A + S, 1 Acro 50 1 μm + 1 Spiral cap 0.2 μm.

experimenters have been able to produce laminar flows in tubes at higher values of *Re* (up to 100 000) and it is apparently impossible to find a universal critical value of *Re* for flows in tubes (Monin and Yaglom, 1971). Consequently it is difficult to characterize, with certainty, the flow regime in each system. Anyway, the problem is not critical provided that adequate corrections for high frequency losses are applied. These corrections are discussed in section V.D.2).

To prevent condensation, in most cases the air is sucked through the tube and the analyser (i.e. the air pump is the last link in the air transport chain). The data are then corrected for the effect of under-pressure within the analyser's sample cell (Figure 2a) (Moncrieff *et al.*, 1997a). A sensor (LI-COR 6262-03) that measures the IRGA chamber pressure at 1 Hz may be used to that end. Another possibility (SW1 and 2) is to blow the air through the analyser, giving high flow rates and a reduced number of corrections. With a suitable air pump and appropriate heating, pump-induced distortions and condensation can be prevented more effectively (Grelle, 1997). A third possibility is to transport the air at a high flow rate close to the measurement point with subsampling at a lower flow rate for H_2O and CO_2 (Figure 2b). This method produces very high flow rates without creating too large an under-pressure in the measuring chamber, but it requires two pumps. It is used in long tube systems (DK1, GE2).

To prevent contamination of the IRGA chamber, filters must be placed upstream of the analyser. Except for sites with very clean air (FI1), a number of filters placed in series is required to reduce the zero drift of the analyser that becomes inevitable after a couple of months. It is therefore recommended to place two filters in series in the pumping circuit. The first filter (ACRO 50 PTFE 1 μm; Gelman, Ann Arbor, Michigan, USA) should be placed at the inlet of the tube and replaced every fortnight (more frequent changes have been necessary in winter at some sites when reduced mixing conditions produces an acceleration in filter contamination (FR1, BE1)). The second filter (ACRO 50 PTFE 1 μm, or Spiral cap 0.2 μm; Gelman) may be placed close to the analyser and does not need to be changed as frequently. The positioning of a filter at the inlet of the tube also prevents contamination of the tube by hygroscopic dirt which could damp the high-frequency water vapour fluctuations and so lead to under-estimation of water vapour flux (Leuning and Judd, 1996). In sites near oceans (FR2), sea salt could damage the IRGA chamber coating. To avoid such problems a coalescent filter (Balston A944) is placed at the input of the IRGA chamber.

The time lag that is introduced in a ducted system is taken into account by software, and the lag varies significantly from site to site according to tube length and flow rate. The exact determination of the time lag is more crucial for systems with long tubes (DK1). The dominant parameter determining time lag is the flow rate through the sample tube (Leuning and Moncrieff, 1990) and the filters. Thus, if some sort of flow regulator is used, the time lag is kept

fairly constant; otherwise, a dynamic correction must be applied. Generally, the time lag is computed by finding the maximum in the covariances (McMillen, 1988; Grelle and Lindroth, 1996; Moncrieff *et al.*, 1997a) and is 1–2 s higher than that predicted by flow equations in the tube. The difference between theory and practice arises because the fluid flow equations do not take into account the influence of the filters and the time constant of the analyser. In practice, however, time lag variations are usually small and can be specified in the software within a range of ± 1 s of the true lag. This permits faster computation and a reduction in errors, especially when the fluxes are low and the maximum in the covariance is difficult to detect.

To enable automatic calibration of the CO_2 signal, a calibration gas can be supplied to the gas analyser at predetermined intervals through a remotely controlled solenoid valve. Reference H_2O sources such as the LI-COR dewpoint generator are not suitable for unattended long-term use and high flow rates. Thus, separate measurements of reference air humidity are more appropriate to ensure calibration of the H_2O signal.

E. Tower Instrumentation

Given the aim of operating flux systems for extended periods of time, some protection of the system components from adverse weather is essential. Owing to the large climate variability between the different EUROFLUX sites, the technical requirements for appropriate protection differ. At northern latitudes (SW1 and 2, FI1), the air analysis system is placed in thermally insulated boxes which are ventilated by filtered air and heated to keep the internal temperature constant (Grelle, 1997). In some cases, the sonic probes are heated to prevent rime (SW1 and 2, GE1, FI1). In the Mediterranean region, it is generally sufficient to keep the system in a clean and dry environment.

The signals of air temperature, water vapour concentration, CO_2 concentration, gas analyser temperature, and air flow through the analyser are connected to the sonic's A/D converter. Here, the non-linear signals of the gas analyser offer the fastest frequency response, whereas the linearized outputs offer higher signal resolution when used with the Solent sonic anemometer's built-in A/D converter. The limitation in frequency response is larger for the H_2O signal, whereas in practice the limited resolution affects only the CO_2 signal (Grelle, 1997). Thus, utilization of the linear CO_2 signal and the non-linear H_2O signal is the optimum configuration. Signals from the sonic anemometer are transferred by serial communication according to the RS 422 standard.

The power supply and interface unit originally delivered with the SOLENT sonic does not have electrically insulated signal lines and it has only single-ended inputs using the same reference potential as the sonic probe itself. In particular, this means that, if additional devices with a different reference potential (e.g. the LI-COR gas analyser) are connected to the sonic in the

original configuration, differences in ground potential between the mast and the ground can cause currents through the signal lines and thus data errors. To overcome this problem and to improve the lightning protection, the anemometer has been modified by one group (SW1 and 2), which now uses a floating power supply and a modified converter interface with insulated signal lines (Grelle and Lindroth, 1996). Another group (FI1) uses optical fibres to transfer the data from the tower to the measurement building at the bottom of the instrumentation tower. This requires a modification of the Solent output (Haataja and Vesala, 1997).

IV. ADDITIONAL MEASUREMENTS

At each EUROFLUX site, the eddy covariance measurements are supported by a set of meteorological measurements that are also collected every half an hour. The role of these measurements is:

(1) To characterize the meteorological conditions under which fluxes occur. This allows further analysis as the inference of the flux responses to meteorological variables (at a half-hourly scale) or the response of the annual carbon sequestration to climate and the interpretation of the interannual variability of the net carbon storage.
(2) To correct the eddy covariance measurements. In particular, the CO_2 storage estimation (term III in equation (2)) requires half-hourly measurements of the CO_2 concentration below the measurement point; corrections of fluxes for pressure or for high-frequency losses require additional meteorological measurements.
(3) To control the quality of the measurements. The energy balance closure test is performed currently to check the data quality (see section VI.D). It requires, in particular, the net radiation and the energy storage.
(4) To provide a set of prognostic data that can be used to fill in the gaps in the flux data series (see section IX).
(5) To provide a set of input data for Soil Vegetation Atmosphere Transfer (SVAT) models that can be used for calibration as well as for validation.

The list of variables that are measured at all sites is given in Table 3.

V. DATA ACQUISITION: COMPUTATION AND CORRECTION

A. General Procedure

The general procedure followed to collect and process the data is presented in Figure 3.

At intervals of 1/20.8 s, instantaneous measurement of values for the three components of the wind velocity, the speed of sound and the molar fractions of

Table 3
Meteorological variables measured in the EUROFLUX sites

Symbol	Unit	Variable	Instrument	Status
Radiation				
R_g	W m^{-2}	Global radiation	Pyranometer	O
R_n	W m^{-2}	Net radiation	Net radiometer	O
PPFD	μmol m^{-2} s^{-1}	Photosynthetic photon flux density	Photodiode	O
R_{ref}	W m^{-2}	Reflected radiation	Pyranometer	F
R_d	W m^{-2}	Diffuse radiation	Pyranometer + screen	F
APAR		Light interception	Photodiodes	F
Temperature				
T_a	°C	Air temperatures (profile)	Resistance or thermocouple	O
T_{bole}	°C	Bole temperature	Resistance or thermocouple	O
T_s	°C	Soil temperature (profile 5–30 cm)	Resistance or thermocouple	O
T_c	°C	Canopy radiative temperature	Infrared sensor	F
G	W m^{-2}	Soil heat flux density	Heat flux plates	O
Hydrology				
P	mm	Precipitation	Rain gauge	O
RH	%	Relative humidity profile	Resistance, capacitance or psychrometer	O
SWC	% by volume	Soil water content (0–30, 40–70, 80–110)	TDR or theta probe (15 days)	O
SF	mm	Stemflow	Tree collectors (15 days)	F
T_f	mm	Throughfall	Pluviometer (15 days)	F
SNOWD	mm	Snow depth	Sensor (15 days)	F
Miscellaneous				
P_a	kPa	Pressure	Barometer	O

O, obligatory; F, voluntary.

CO_2 and water vapour is collected and stored. Software computes the mean values, variances, covariances and the so-called 'uncorrected fluxes' at this stage, corrections for high-frequency losses are not performed). The software that performs these computations is described in section V; the operations performed and the recommended equations are given in section V.B; the software intercomparison exercise, carried out among EUROFLUX teams, is presented in section V.C; and the difference between different high-pass filtering methods is discussed in section V.D.1.

The amount of raw data collected at these sample rates is about 600 Mb per month and is typically stored on tapes, compact disk or removable drives for post-processing (e.g. further analysis of the time series, data quality analysis or spectral analysis). The supporting meteorological measurements are also averaged over intervals of half an hour. In particular, energy storage in the biomass and air (possibly in the soil) or CO_2 storage in the air is computed at

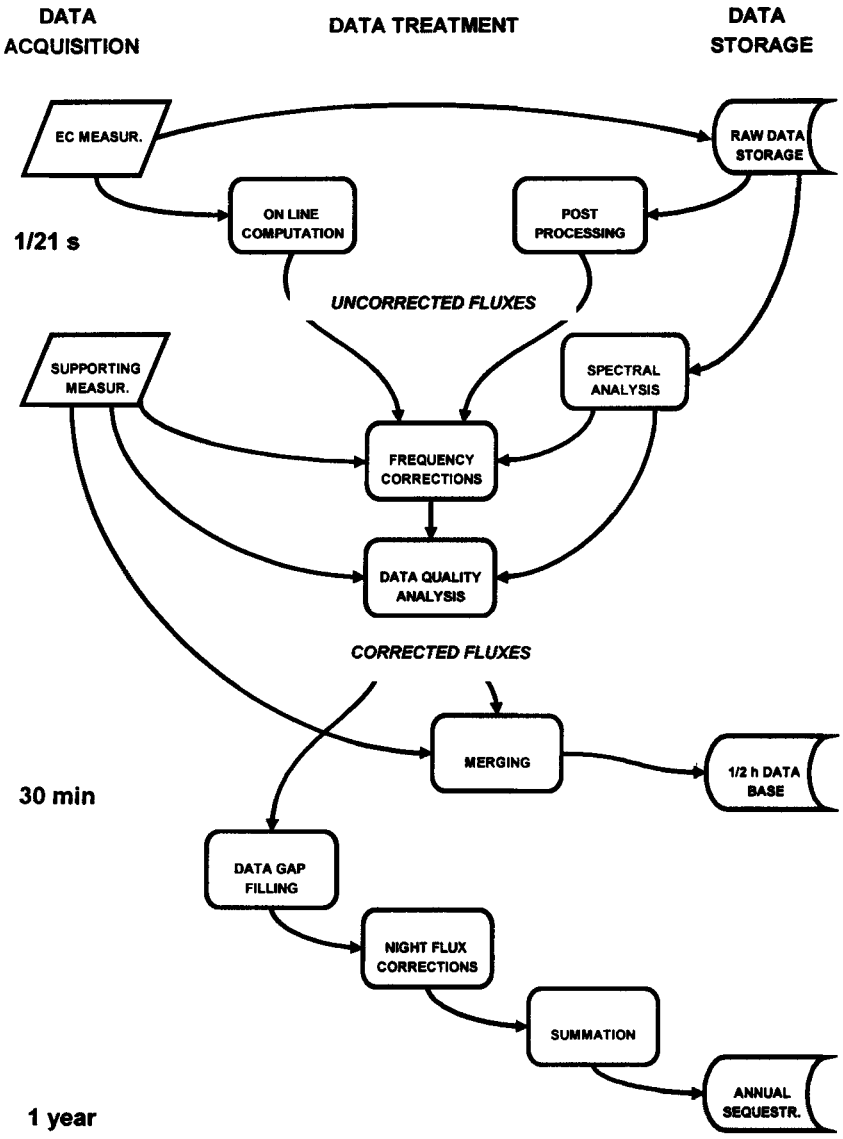

Fig. 3. Schematic of data acquisition, processing and storage in EUROFLUX systems.

this stage. Meanwhile, the corrections of fluxes are applied. They include corrections for latent heat or lateral momentum fluxes (Schotanus *et al.*, 1983) and corrections for high-frequency losses (Moore, 1986; Leuning and Judd, 1996; Moncrieff *et al.*, 1997a). The latter require the cut-off frequency of the system that can be obtained by spectral analysis. The procedure is described in section V.D.2. There is no need for air density corrections on the CO_2 flux (Webb *et al.*, 1980), as will be shown below.

The eddy covariance fluxes are then submitted to a series of tests to eliminate data that fail certain criteria. Different tests (based on statistical analysis, stationarity or similarity criteria, energy balance closure) are presented in section VI. After correction and quality analysis, the eddy covariance and supporting measurements are merged and constitute the input from each group to the EUROFLUX database.

At a yearly time scale, the fluxes are summed to provide an annual carbon sequestration estimation. This sum requires a complete data series, i.e. a procedure to fill in the unavoidable gaps in the flux data. A procedure based on neural networks is described in section IX. The errors that affect the annual sequestration are discussed later: the selective systematic error due to underestimation of the fluxes at night is discussed in section X and the other measurement uncertainties are discussed in section XI.

B. Half-hourly Means, (Co-)variances and Uncorrected Fluxes

1. Computation of the Means and Second Moments

The input data are the instantaneous values of the three components of the velocity (u, v, w (ms^{-1})), of the sound speed (U_{son}(ms^{-1})), and of the CO_2 and H_2O mole fractions (c(μmol mol^{-1}), h (mmol mol^{-1})). In the following part, variables may be designed in a general way by ξ or η, and a scalar concentration by s.

The mean of ξ and the second moment of ξ and η are computed as:

$$\overline{\xi} = \frac{1}{n_s} \sum_{k=1}^{n_s} \xi_k \tag{5}$$

and

$$\overline{\xi'\eta'} = \frac{1}{n_s} \sum_{k=1}^{n_s} \xi'_k \eta'_k \tag{6}$$

where n_s is the number of samples. The fluctuations (ξ_k') around the mean at the step k ($\overline{\xi_k}$) are computed as:

$$\xi'_k = \xi_k - \overline{\xi}_k \tag{7}$$

In autoregressive filtering algorithms, the mean $\bar{\xi}_k$ is computed as (McMillen, 1986, 1988; Baldocchi *et al.*, 1988; Kaimal and Finnigan, 1994):

$$\bar{\xi}_k = e^{-\Delta t/\tau_f}\bar{\xi}_{k-1} + (1 - e^{-\Delta t/\tau_f})\xi_k \tag{8}$$

where Δt is the measurement time interval and τ_f is the running mean time constant. As $\Delta t << \tau_f$, equation (8) may also be written (after first-order Taylor expansion):

$$\bar{\xi}_k = \left(1 - \frac{\Delta t}{\tau_f}\right)\bar{\xi}_{k-1} + \frac{\Delta t}{\tau_f}\xi_k \tag{8'}$$

It is to be noted that the running mean $\bar{\xi}_k$ cannot be taken for the mean $\bar{\xi}$, which is computed on the whole data set.

In linear detrend algorithms, ξ_k is computed by least squares regression as (Gash and Culf, 1996):

$$\bar{\xi}_k = \bar{\xi} + b\left(t_k - \frac{1}{n_s}\sum_{k=1}^{n_s} t_k\right) \tag{9}$$

where t_k is the time at the step k and b is the slope of the linear trend of the sampling. It is computed as:

$$b = \frac{\sum_{k=1}^{n_s}\xi_k t_k - \frac{1}{n_s}\sum_{k=1}^{n_s}\xi_k \sum_{k=1}^{n_s} t_k}{\sum_{k=1}^{n_s} t_k t_k - \frac{1}{n_s}\sum_{k=1}^{n_s} t_k \sum_{k=1}^{n_s} t_k} \tag{10}$$

Non-linear transformations of the variables must be applied before any mean or second moment computation. This is the case with the sonic temperature T_{son} (K) which is deduced from sound velocity (U_{son}) by (Schotanus *et al.*, 1983; Kaimal and Gaynor, 1991):

$$T_{son} = \frac{U_{son}^2}{403} \tag{11}$$

For the computation of $\overline{w'c'}$ or $\overline{w'h'}$, the time series of w_k' must be delayed for synchronization with c_k' or h_k' to take into account the time taken for the air to travel down the sample tube. Recommendations concerning the time lag computation were given in section III.C. Some algorithms in use within EUROFLUX (SW1 and 2) use a constant time lag, whereas others (e.g. EdiSol) estimate it by maximization of the covariances.

2. *Co-ordinate rotation*

Co-ordinate rotations are applied on the raw means and second moments. The first two-axis rotation aligns u parallel to the mean wind velocity, and nullifies v and w. Its aim is to eliminate errors due to sensor tilt relative to the terrain surface or aerodynamic shadow due to the sensor or tower structure. However, it always suppresses the vertical velocity component and that is not always appropriate as non-zero vertical velocity components may appear above tall vegetation when flux divergence or convergence occurs (Lee, 1998).

The two-axis co-ordinate change on mean velocity components and on covariances, including scalar concentrations, may be expressed in matrix form (McMillen, 1986; Kaimal and Finnigan, 1994; Grelle, 1996):

$$\begin{aligned} \overline{u_{2,i}} &= \sum_j A_{02,i,j} \cdot \overline{u_{0,j}} \\ \overline{s'u'_{2,j}} &= \sum_j A_{02,i,j} \cdot \overline{s'u'_{0,j}} \end{aligned} \tag{12}$$

where the numerical index (n) refers to the number of rotations applied to the means and covariances, $A_{02,i,j}$ are the elements (ith line, jth column) of the two-axis rotation matrix and $u_{n,j}$ is the jth element of the velocity vector. In particular, the mean wind speed is $U = \overline{u_{21}}$. The expression of A_{02} in terms of the non-rotated velocity components is established in Appendix A and given in equation (A4).

The two-axis rotation is applied on the variances and covariances following:

$$M_2 = A_{02} M_0 A_{02}^{\tau} \tag{13}$$

where A_{02}^{τ} is the transposed A_{02} and M_n are the (co)variance matrices defined as:

$$M_n = \begin{pmatrix} \overline{u'_n u'_n} & \overline{u'_n v'_n} & \overline{u'_n w'_n} \\ \overline{v'_n u'_n} & \overline{v'_n v'_n} & \overline{v'_n w'_n} \\ \overline{w'_n u'_n} & \overline{w'_n v'_n} & \overline{w'_n w'_n} \end{pmatrix} \tag{14}$$

The third rotation is performed around the x-axis in order to nullify the lateral momentum flux density ($\overline{v'w'}$ covariance). Indeed this term is zero over plane surfaces and is likely to be very small over gentle hills. A complete justification on this point is given by Kaimal and Finnigan (1994). McMillen (1988) stresses that this rotation is not well defined in low-speed conditions and recommends

its application with care and, in any event, to limit it to 10°. The co-ordinate change for means and covariances including a scalar is expressed by:

$$\begin{aligned} \overline{u_{3,j}} &= \sum_j A_{23,i,j} \cdot \overline{u_{2,j}} \\ \overline{s'u'_{3,j}} &= \sum_j A_{23,i,j} \cdot \overline{s'u'_{2,j}} \end{aligned} \tag{15}$$

The expression of A_{23} in terms of the two-axis rotated velocity components is established in Appendix B (equation (B4)). For the variances and the covariances, the change of co-ordinates is:

$$M_3 = A_{23} M_2 A_{23}^{\tau} \tag{16}$$

Since computation of the A_{23} matrix elements requires two rotated variances and covariances computations, it is not possible to combine A_{23} and A_{02} to build a unique three-axis rotation matrix. In the following sections, the three components of the three-axis rotated instantaneous velocity will be noted, for simplicity, *u*, *v* and *w*.

3. Conversions and Corrections

The mean air temperature $\overline{T}_a$ (K) is deduced from sonic temperature using (Schotanus *et al.*, 1983; Kaimal and Gaynor, 1991):

$$\overline{T}_a = \frac{\overline{T}_{son}}{1 + 3.210^{-4} h} \tag{17}$$

The fluxes of CO_2 (F_c, μmol m^{-2} s^{-1}) or H_2O (F_w, mmol m^{-2} s^{-1}) are directly deduced from the rotated covariances as:

$$F_s = \frac{P_a}{\Re \overline{T}_{son}} \overline{w's'} \tag{18}$$

where P_a is atmospheric pressure and $\Re$ is the gas constant (8.314 J K^{-1} mol^{-1}).

A paper by Webb *et al.* (1980) pointed out the necessity to correct eddy covariance fluxes in order to remove air density fluctuations. These fluctuations, due either to temperature or to water vapour concentration fluctuations, can be erroneously attributed to fluctuations in scalur concentrations. The correction term was computed for closed path by Leuning and Moncrieff (1990) and Leuning and King (1992). They showed that, if the air was brought in the chamber at a constant temperature, the density corrections due to

temperature fluctuations could be removed. Leuning and Judd (1996) estimated the minimum sampling tube length required to reach such constant temperature when the tube is made by a good thermal conductor. Rannik *et al.* (1997) developed a similar computation for poor thermal conductors like Teflon, which is currently used in standard eddy covariance systems. They showed that the minimum tube length to reduce fluctuations to a fraction of 0.01 from the initial temperature is of the order of 1000 times the tube inner diameter, a length reached in most of the experimental set-ups. They concluded that there is no need to apply the density correction due to sensible heat flux. In addition, as humidity fluctuations are automatically corrected by the LI-COR software, there is no need to apply the density corrections due to latent heat flux either.

The latent heat flux is defined as $\lambda M_w F_w / 1000$ where M_w is the molar mass of water (0.0180153 kg mol^{-1}) and λ (J kg^{-1}) is the latent heat of vaporization of water, which varies with air temperature:

$$\lambda = (3147.5 - 2.37T_a)10^3 \tag{19}$$

Finally, the sensible heat flux, H, is given as:

$$H = \rho_m C_m \overline{w'T_a'} = \frac{P_a M_d}{\Re \bar{T}_{son}} C_d \left(\overline{w'T'_{son}} - 3.210^{-4} \bar{T}_{son} \overline{w'h'} + \frac{2U\overline{u'w'}}{403} \right) \tag{20}$$

where M_d is the molar mass of dry air (0.028965 kg mol^{-1}), ρ_m and C_m are the density and specific heat of the moist air (which is practically the same for humid and dry air, i.e. less than 0.5% difference in the meteorological range). The second term in parentheses accounts for the difference between sonic and real temperature (see equation (17)), the third term corrects the sound speed for lateral momentum flux perturbations (Schotanus *et al.*, 1983; Kaimal and Gaynor, 1991). Equation (20) is rigorous only when the speed of sound is measured along a vertical sound path. Thus, in the case of the SOLENT, where the axis is tilted with respect to the vertical, this relation is not strictly valid. However, the departure from this relation is small. When the temperature fluctuations are measured with a fast thermometer (platinum resistance wire), these corrections are not necessary.

C. Intercomparison of Software

Although common software for data acquisition and flux computation was proposed, several teams within EUROFLUX opted to develop their own software in order to retain flexibility and to be able to adapt the software for particular instrumentation configurations (e.g. simultaneous monitoring of

several eddy covariance systems). As one of the main objectives of EUROFLUX is to perform comparisons among sites, it was necessary to ensure that the differences in measured flux from site to site was not an artefact of the different algorithms in use. An intercomparison between the available software was therefore carried out.

First, a series of raw data files ('golden files') obtained from a standard eddy covariance system was established. This data set comprises 19 successive 30-min digital files containing raw time-series data from the sonic anemometer, namely the three velocity components, speed of sound (all ms^{-1}), CO_2 (μmol mol^{-1}) and H_2O concentrations (mmol mol^{-1}) sampled at 20.8 Hz. The data cover a range of meteorological conditions, at night and during the day, and were obtained at the BE1 site on 1 June 1997 between 12.00 and 9.00 p.m. (The 'golden files' are available on fsagx.ac.be\ftp\euroflux\serie2.zip). A description of this site is given by Aubinet *et al.* (unpublished).

Each software package was run independently on this data set and the results were compared. When convergent, they were considered as standards (available on fsagx.ac.be\ftp\euroflux\results.xls) and the maximum difference between them as the tolerance. Six software packages were used to generate the standards; three used a running mean algorithm with a 200-s time constant: *EdiSol* (Edinburgh University, UK), *UIA* (University of Antwerpen, Belgium) and *SMEAR Solent* (University of Helsinki, Finland), and the other three used a linear detrending algorithm *UBT* (University of Bayreuth, Germany), *RISOE* (RISOE National Laboratory, Denmark) and *IBK* (Georg August University of Goettingen, Germany). All of them output the means and variances of wind velocity (three components), temperature, water vapour and CO_2 concentrations, the fluxes of momentum (or the friction velocity), sensible heat, water vapour (or latent heat) and CO_2.

All software packages were in very good agreement for mean values: the maximum difference between them was 1% for wind velocity, 0.01% for CO_2 concentration and 0.03% for the water vapour concentration. The agreement for software using either linear detrend or running mean was better than 2% for the latent heat and better than 1% for the other fluxes.

The main sources of disagreement between software were:

(1) Individual errors: some programming errors were detected as a result of this exercise, which fully justifies it. This test is thus recommended for each software designer.
(2) Differences in software initialization for running mean algorithm: the initialization period of these algorithms may exceed the time constant by a factor of 5 or 6. Under these conditions, the first measurement of any series generally gives poor flux agreement. An ideal initialization procedure would be to process the first series of data in the reverse order and initialize with the running mean obtained then. This is impractical, of course, for on-line measurements.

(3) Time lag estimations: software optimizing the time lag without restricting its variation range biased (up to 50% underestimation) the flux values during some periods when the correlation optimum was not clearly defined.
(4) Differences between the hypotheses used for the computation: to avoid such divergence, the use of a standard set of hypotheses and equation is recommended. In EUROFLUX, we used the equations presented in section V.B.1.
(5) Differences between linear detrend and running mean algorithms reached 10% and flux estimates were generally higher for software employing the running mean algorithm. However, the present data series is too short to lead to a definitive conclusion.

D. Correction for Frequency Response Losses

The turbulent flow in the atmospheric boundary layer may be considered as a superposition of eddies of different sizes. At one measurement point they generate velocity and scalar concentration fluctuations of different frequencies. It is common to describe the frequency repartitions of the fluctuations by introducing the co-spectral density. In the case of turbulent fluxes of a scalar, the co-spectral density, C_{ws} is related to the covariance (Stull, 1988; Kaimal and Finnigan, 1994):

$$\overline{w's'} = \int_0^\infty C_{ws}(f)\,df \tag{21}$$

where f is the cyclic frequency. In practice, the integral range is limited at low frequency by the observation duration and/or the high-pass filtering, and at high frequency by the instrument response. Consequently, the measured turbulent fluxes of a scalar s may be thought of as the integration over frequencies of the co-spectral density multiplied by a transfer function characterizing the measurement process:

$$\overline{w's'_{\text{meas}}} = \int_0^\infty TF(f)\,C_{ws}(f)\,df \tag{22}$$

The fluxes must therefore be corrected to take these effects into account. A correction factor is introduced which is the ratio of the flux free from filtering (equation (21)) and the measured flux (equation (22)):

$$CF = \frac{\int_0^\infty C_{ws}(f)df}{\int_0^\infty TF(f)C_{ws}(f)df} = \frac{\int_0^\infty C_{ws}(f)df}{\int_0^\infty TF_{\text{HF}}(f)TF_{\text{LF}}(f)C_{ws}(f)df} \tag{23}$$

where the low (TF_{LF}) and high (TF_{HF}) frequency parts of the transfer function are introduced separately.

1. Effect of High-pass Filtering on Fluxes

As shown in section V.B.1, turbulent fluxes of scalars are calculated over a finite averaging time as the average products of the fluctuations of vertical wind speed and scalar concentration, obtained from the original records by linear detrending (LD) or high-pass running mean filtering (RM). The transfer functions for linear detrending and high-pass filtering generally remove variability (also covariance) at low frequencies, passing the high-frequency contribution. The spectral transfer functions for variances and covariances due to LD and RM are (Kristensen, 1998):

$$TF_{LF}^{LD}(f) = 1 - \frac{\sin^2(\pi f t_c)}{(\pi f t_c)^2} - 3\frac{\left(\frac{\sin(\pi f t_c)}{\pi f t_c} - \cos(\pi f t_c)\right)^2}{(\pi f t_c)^2} \qquad (24)$$

$$TF_{LF}^{RM}(f) = \frac{(2\pi f t_f)^2}{1+(2\pi f t_f)^2}$$

where τ_c is the time period of the trend calculation and averaging, and τ_f is the time constant of the high-pass filter. In the case of the RM method, it is assumed that high-pass filtered series are used directly as the fluctuating components in the flux calculation. The high-pass filtering effect of the LD method depends on the time interval, τ_c, but the effect of the RM depends only on the time constant of the filter, τ_f. Because the transfer functions are less than unity at low frequencies, application of LD or RM in flux calculation leads to systematic underestimation of turbulent fluxes.

The filtering effect of the RM with a time constant 200 s is stronger than that of LD (Figure 15 in Kristensen, 1998), where the curve of high-pass filtering for $\tau_f/\tau_c = 60^{-1/2}$ corresponds roughly to a running mean with a time constant of 200 s. In other words, the absolute average flux estimates obtained by RM with a time constant of 200 s, with negligible random uncertainty due to the stochastic nature of turbulence, are always less than the estimates obtained when applying the LD algorithm. This is not necessarily valid for the short-period average fluxes with significant random errors, being calculated from a realization of turbulence in virtually a point in space over a relatively short time.

Due to detrending or high-pass filtering, estimated average fluxes are always biased. For the unstable, but neutral limit of the atmospheric surface

layer co-spectra given in Horst (1997), the systematic errors of flux estimates due to LD and RM with time constant 200 s for the height to wind speed ratios from 1 to 10, vary from 0.7 to 6.1% and from 1.5 to 11.4% (without taking into account the underestimation of fluxes at high frequencies) respectively. The corresponding error range for the RM with time constant 1000 s is from 0.2 to 1.8%. The systematic errors are bigger for unstable conditions and smaller for stable conditions. The relatively small errors in short-period fluxes translate to bigger errors in long-term averages. The systematic errors of fluxes can be minimized by choosing a suitable filtering method or averaging time, but there are also other factors which should be accounted for when choosing the filter for calculation of statistics.

To observe negligible systematic errors in fluxes, the RM has to be applied with moderately long time constants, but this leads to systematic overestimation of variances in the periods of non-stationarity of first moments (Shuttleworth, 1988). In addition, it was shown by Rannik and Vesala (1999.) that fluxes are subject to increased random errors during episodes of non-stationarity. Thus, it seems justified to apply the method with a moderate time constant to avoid these problems at the expense of small systematic errors in fluxes, which should be then accounted for. In the case of atmospheric surface layer measurements, reasonable values of the time constant of the RM seem to be between 200 and 1000 s, probably around 500 s, dependent on the measurement height.

Application of the LD method with commonly accepted averaging times does not generally lead to overestimation of variances and increases in random errors, to the advantage of the method. However, the systematic errors in fluxes due to LD are not negligible under certain experimental conditions. For evaluation of systematic errors, co-spectral information is needed. The model co-spectra of turbulence can be used in the estimation of errors, but there is remarkable uncertainty in the low-frequency co-spectral densities under unstable stratification (Kaimal *et al.*, 1972), when the underestimation of fluxes is greatest. Alternatively, the co-spectra could be estimated as site specific from a series of measurements under similar conditions of atmospheric stability to obtain the low-frequency densities with sufficient accuracy.

2. *Effects of Low-pass Filtering*

Low-pass filtering results from the inability of the system to resolve fluctuations associated with small eddies and induces an underestimation of the measured turbulent flux. The transfer function characterizing the high-frequency losses (TF_{HF}) is 1 at low frequencies, decays to zero at high frequencies and may be characterized by its cut-off frequency (f_{co}), that is, the frequency at which the transfer functions equals $2^{-1/2}$. When the cut-off frequency is known, the transfer function may be combined in equation (23) with the high-pass transfer function (equation (24)) and model co-spectra as

defined by Kaimal *et al.* (1972) or Horst (1997) in order to estimate the correction factor. Moncrieff *et al.* (1997a) showed in this way that, for a given eddy covariance system, the correction factor is a function of wind speed (U) and measurement height above the displacement height ($h_m - d$). We show in Figure 4 the relation between the correction factor and the cut-off frequency for five different $(h_m - d)/U$ values. The correction factor values are listed in Table 4. The transfer function and its cut off frequency may be estimated either theoretically or experimentally. Both approaches will be described here.

The theoretical description of eddy covariance system transfer functions was first given by Moore (1986) for momentum and sensible heat fluxes. It was later applied to scalar flux measurements by Leuning and Moncrieff (1990), Leuning and King (1992), and Leuning and Judd (1996), who treated in particular the systems that use a closed-path gas analyser. A complete description of the transfer functions of eddy covariance systems with closed-path analysers is given by Moncrieff *et al.* (1997a). Following this theory, the transfer function of an eddy covariance system is considered as the product of individual functions, each describing a particular instrumental effect. The instrument effects that damp the high-frequency fluctuations are: the dynamic frequency response of the sonic anemometer and of the IRGA, the sensor response mismatch, the scalar path averaging, the sensor separation (Moore, 1986) and the attenuation of the concentration fluctuations down the sampling tube, which is typical of closed-path systems (Leuning and Moncrieff, 1990; Leuning and King, 1992; Leuning and Judd, 1996).

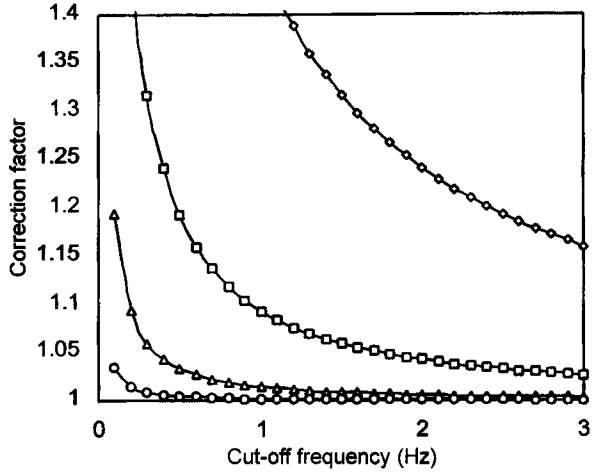

Fig. 4. Evolution of the correction factor according to the cut-off frequency. ◇, $(h_m - d)/U = 0.2$ s; □, $(h_m - d)/U = 1$ s; △, $(h_m - d)/U = 5$ s; ○, $(h_m - d)/U = 25$ s.

Table 4
Correction factor for high-frequency damping in relation to the cut-off frequency (f_{co}) and to the ratio $(h_m - d)/U$

f_{co} (Hz)	$(h_m - d)/U$ (s)			
	0.2	1	5	25
0.1	4.136	1.819	1.194	1.035
0.2	2.742	1.456	1.094	1.015
0.3	2.246	1.316	1.060	1.009
0.4	1.984	1.241	1.043	1.006
0.5	1.819	1.193	1.033	1.005
0.6	1.704	1.160	1.027	1.004
0.7	1.619	1.137	1.022	1.003
0.8	1.552	1.119	1.019	1.003
0.9	1.499	1.105	1.016	1.002
1.0	1.456	1.093	1.014	1.002
1.2	1.388	1.076	1.011	1.001
1.4	1.337	1.064	1.009	1.001
1.6	1.297	1.055	1.008	1.001
1.8	1.266	1.048	1.007	1.001
2.0	1.240	1.043	1.006	1.001
2.2	1.219	1.038	1.005	1.001
2.4	1.201	1.035	1.005	1.001
2.6	1.185	1.031	1.004	1.001
2.8	1.172	1.029	1.004	1.000
3.0	1.160	1.026	1.003	1.000

The first four functions are described in detail by Moore (1986) and will not be restated here. They depend only on the sonic and IRGA characteristics and on the wind speed, and are thus the same for all the EUROFLUX sites. The cut-off frequency of the transfer function that results from the combination of these four effects depends slightly on the wind speed, being 2.26 Hz at 1 ms^{-1} and 3.5 Hz at 5 ms^{-1}. Above 5 ms^{-1}, it remains practically constant. These values correspond to the maximal cut-off frequency that can be achieved in EUROFLUX systems. The resulting error is significant only under high wind speeds or at low measurement height (it exceeds 1% when $U > 2.5$ ms^{-1} at $h_m - d = 4$ m, $U > 4.5$ ms^{-1} at $h_m - d = 8$ m, $U > 7.0$ ms^{-1} at $h_m - d = 12$ m). These effects can be neglected most of the time.

The function describing the sensor separation effect is given by:

$$TF_s(f) = \exp\left\{-9.9\left(\frac{fL_s}{U}\right)1.5\right\} \tag{26}$$

where L_s is the separation distance between the sensors. Its cut-off frequency ($f_{co\text{-}ss}$) is given by:

$$f_{co\text{-}ss} = \frac{0.107U}{L_s} = a_{ss}U \tag{27}$$

It increases linearly with wind speed. The value of the slope of the increase, a_{ss}, is given for each site in Table 2. It varies from 0.2 to 0.9 m^{-1}. The error is thus particularly important at low wind speeds, especially at sites with a L_s, and this distance ought to be kept to a minimum.

The functions describing the attenuation of the fluctuation concentrations down the sampling tube are (Lenshow and Raupach, 1991; Leuning and King, 1992):

$$TF_t(f) = \exp\left\{\frac{-\pi^2 r_t^2 f^2 L_t}{12 D_s U_t}\right\} \tag{28}$$

when the flow in the tubes is laminar, or:

$$TF_t(f) = \exp\left\{\frac{-80 Re^{-1/8} r_t f^2 L_t}{U_t^2}\right\} \tag{29}$$

when it is turbulent. L_t and r_t are the tube length and radius, U_t the air speed in the tube and D_s the molecular diffusivity of the scalar. The argument of the exponentials in equations (28) and (29) are half the values given by Leuning and King (1992) because the latter refer to variance calculations whereas ours refer to covariance calculations. On the other hand, the values given by Moncrieff *et al.* (1997a, p. 610, last two formulae) are too big by a factor of 2. In addition, following a typographic error, the exponent –1/8 was omitted in their last formula.

The corresponding cut-off frequencies ($f_{co\text{-}t}$) are given, respectively, by:

$$f_{co\text{-}t} = 0.649\sqrt{\frac{U_t D_s}{r_t^2 L_t}} \tag{30}$$

in the laminar case, and:

$$f_{co\text{-}t} = 0.666 Re^{1/16} \frac{U_t}{\sqrt{r_t L_t}} \tag{31}$$

in the turbulent case. For the latter, Leuning and Judd (1996) have proposed an alternative expression derived from the work of Massman (1991):

$$f_{co\text{-}t} = \ln(0.76 Re^{0.039}) \frac{U_t}{\sqrt{r_t L_t}} \tag{32}$$

The tubing cut-off frequencies predicted by theory are given for each site in Table 2. The cut-off frequencies are high under a turbulent regime and the tubing effect appears insignificant. On the other hand, under a laminar regime the cut-off may be reduced to 0.4 or 0.5 Hz and thus it becomes the main influence on frequency loss.

In conclusion, the theoretical approach shows that the transfer function depends only on the wind speed and on the system characteristics. In the case of the closed chamber system used in the EUROFLUX network, the most important characteristics are the tube length and diameter, the mass flow in the tubes and the separation distance between the tube inlet and the sonic. However, it will be shown that the cut-off frequencies predicted by the theory are generally overestimated and consequently that the predicted correction is generally underestimated.

Besides the theoretical approach, an experimental procedure may be developed to estimate the transfer functions and correction factors, as follows:

(1) Select a long time period (3 h at least in order to reduce the uncertainties on the low-frequency part of the co-spectra) with sunny conditions in addition that meets both fetch and stationarity criteria (see section VI.B).
(2) Calculate the co-spectra for heat (C_{wT}), and for the scalar (C_{ws} for CO_2 or water vapour).
(3) Calculate the transfer function as the ratio of the normalized co-spectral densities as:

$$TF_{\mathrm{HF}}^{\mathrm{exp}}(f) = \frac{N_T C_{ws}(f)}{N_s C_{wT}(f)} \tag{33}$$

where N_T and N_s are normalization factors.
(4) Calculate the correction factor by fitting an exponential regression, i.e.:

$$TF_{\mathrm{HF}}(f) = \exp\left\{-0.347\left(\frac{f}{f_{\mathrm{co}}}\right)^2\right\}$$

on the experimental transfer function and introducing it in equation (23).

The normalization factors N_T and N_s should be the real covariances (respectively $\overline{w'T'}$ or $\overline{w's'}$) or, if similarity between heat and scalar transport is assumed, the real standard deviation (respectively σ_T and σ_s). However, the measured covariances and standard deviations are lower than the real ones, as affected by the high-frequency attenuation. To avoid this bias, an alternative way of computing the normalization factor is:

$$\frac{N_T}{N_s} = \frac{\int_0^{f_0} C_{wT}(f)df}{\int_0^{f_0} C_{ws}(f)df} \tag{34}$$

where f_0 is a limit frequency, chosen to be low enough for the attenuation be negligible in the integrals in equation (34), but high enough for the number of points used to estimate the integrals to be sufficient and the uncertainty on the normalization factors to be low.

The co-spectra for sensible heat (the denominator of equation (33)) are obtained experimentally and are therefore affected by the dynamic response of the sonic (or the high-frequency (HF) thermometer), the scalar path averaging and the sensor response mismatch. As the corresponding functions are not the same for the sonic or the HF thermometer and the IRGA, these effects are not taken into account correctly by the experimental transfer function. However, we showed above that these effects were small compared with the tubing or with the sensor separation effect, and could be neglected.

It was shown above that the transfer function depends only on the set-up. Consequently, it is not necessary to calculate it every time. An estimation every month in order to follow the wear of the pumps (if the flow is not controlled) is sufficient.

Aubinet *et al.* (unpublished) followed this method and found significantly lower cut-off frequencies than predicted by theory. The comparison between the theoretical and the experimental transfer function they found for their site is given in Figure 5. They found f_{co} = 0.2 Hz for the experimental transfer function, whereas the theoretically predicted value was 0.6 Hz. Consequently, the theoretically predicted error was half the observed value. In addition, the experimental cut-off frequencies are always lower for water vapour than for CO_2, which cannot be explained only by the differences in molecular diffusivities in equation (28).

Reasons for these discrepancies may come from uncertainties in the mass flow in systems that do not employ a mass flow controller, or from uncertainties in the real mass flow regime, the Reynolds number not being a sufficient criterion, as discussed in section III.D. The main reason is likely to be that the theory ignores the impact of the filters on the transfer function. This effect is significant, depends on the filter type and number (increasing with the filtration surface) and may be higher for water vapour than for CO_2, the former being absorbed and released by the filters. For these reasons, it is recommended: (1) to use the experimental procedure to obtain the transfer function and its cut-off frequency; and (2) to deduce the correction factor from the cut-off frequency, wind velocity and measurement height, using the results of Figure 4 or Table 4.

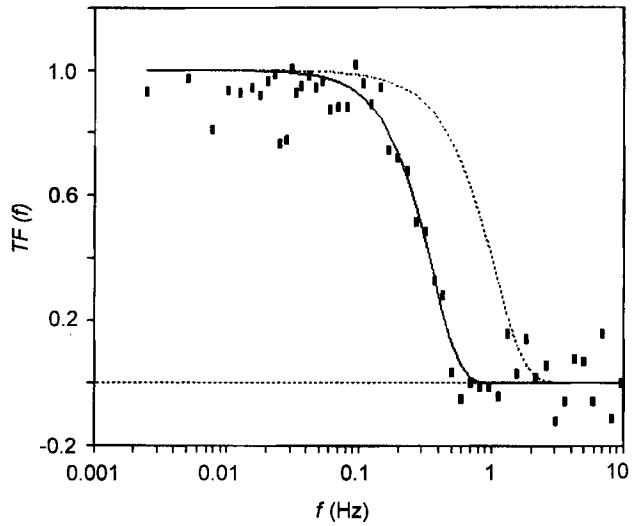

Fig. 5. Comparison between the theoretical (dotted line) and experimental (points and solid line) transfer functions (TF) of the Vielsalm measurement system.

VI. QUALITY CONTROL

To be able to compare the results of different flux measurement stations, the quality of the flux data has to be assessed, because otherwise individual flux patterns cannot be distinguished from site-specific influences of the methodology. However, the quality of flux measurements in the atmospheric boundary layer is difficult to assess, because no standard methods are available to calibrate a given experimental design. There are various sources of errors in flux measurements, ranging from failure to satisfy any of a number of theoretical assumptions to failure of the technical set-up. The resulting errors may be systematic and/or randomly distributed (Moncrieff *et al.*, 1996). Conflicts with the assumptions made in the derivation of the turbulent flux equation arise for certain meteorological conditions and site properties. A more detailed description is given by Moncrieff *et al.* (1997a) and Ibrom *et al.* (unpublished). As these effects cannot be quantified solely from eddy covariance data, a classical error analysis and error propagation will remain incomplete. The alternative chosen here is to investigate empirically whether the fluxes meet certain plausibility criteria.

Four criteria are investigated here. They concern, respectively, the statistical characteristics of the raw instantaneous measurements (section VI.A), the stationarity of the measuring process (section VI.B), boundary layer similarity (section VI.C) and energy balance closure (section VI.D).

A. Raw Data Analysis

The quality control of raw instantaneous data may be performed using a software package (QC) which applies a series of statistical tests as described by Vickers and Mahrt (1997). The FORTRAN package is freely available (http://mist.ats.orst.edu/Software/qc/qc.html) and is intended as a safety net to identify instrument and data-logging errors before data analysis. The user may select which tests are run, limits and thresholds for flagging of data by each test, and local averaging scales. Only the tests that we recommend are described here, including spikes, higher moment statistics, absolute limits and discontinuities. The tests (in italics), described briefly below, warn of suspect data.

Spikes can be caused by random electronic spikes or sonic transducer blockage (during precipitation, for example). An algorithm similar to that described by Højstrup (1993) detects and removes spikes, replacing them with the expected value (based on a local averaging scale and point-to-point autocorrelation) before analysis by the other QC tests. A warning is noted (flagged) when the percentage of replaced data exceeds a threshold. Data are further required to fall within *absolute limits* and normal ranges of *skewness* and *kurtosis*. Discontinuities in the mean and variance of a time series (coherent on a local averaging scale) are detected using the Haar transform (Mahrt, 1991). Finally, each variable is tested for a lower limit in *absolute variance* and a variance ratio for consecutive local windows.

The QC package was run on all 1997 eddy covariance data from BE2 site. Some 13% of all data records were flagged for some problem or another; many appeared to be associated with plumbing problems for LICOR sampling, or with precipitation on the sonic anemometer. Visual inspection confirmed that flagged data were in fact bad (obvious non-physical behaviour in time series, due to instrument, logger or computer problems). No effort was made to evaluate data that were not flagged. For the flagged data, the breakdown by variable is as follows: 10% for u, 16% for v, 13% for w, 19% for T_{son}, 19% for c, and 24% for h. Sixty-nine per cent of the bad data were flagged by more than one QC test; 27% of the flags were due to the absolute limits test. The remaining bad data were flagged by the following individual tests: kurtosis (3%), Haar tests (1%), spikes (< 1%).

Computation of fluxes using bad data generally leads to the addition of random noise. The effects of such noise on long-term Flux estimates have not been quantified. However, it is clearly desirable to minimize problems associated with bad data, and the QC program is an objective means of achieving this goal.

B. Stationarity Test

One hypothesis used to simplify equation (2) is the stationarity of the measuring process. This assumption has to be fulfilled for using the eddy covariance method.

The non-stationarity test has been used since the 1970s by Russian scientists (Gurjanov *et al.*, 1984; see Foken and Wichura, 1996) and is based on equation (6) for the determination of fluxes. The measured time series of about 30-min duration will be divided into $n_s/m = 4 \ldots 8$ intervals of about 5 min. The covariance of a measured signal ξ and η (similar algorithm for dispersions with $\xi = \eta$) of the interval l with $m = 6000$ (6000 measuring values in 5 min for 20-Hz scanning, i.e. $n_s = 36\,000$ in 30 min) measuring values is:

$$\overline{\xi'\eta'} = \frac{1}{m-1}\left[\sum_{k=1}^{m} \xi_{kl}\eta_{kl} - \frac{1}{m}\left(\sum_{k=1}^{m} \xi_{kl}\right)\left(\sum_{k=1}^{m} \eta_{kl}\right)\right] \tag{35}$$

For the test, the mean covariance of the n_s/m single intervals is used:

$$\overline{\xi'\eta'} = \frac{1}{n_s/m}\left[\sum_{l=1}^{n_s/m} \overline{\xi'_l\eta'_l}\right] \tag{36}$$

On the other hand, the value of the covariance for the full period will be determined according to (compare with equation (35)):

$$\overline{\xi'\eta'} = \frac{1}{n_s-1}\left[\sum_{l=1}^{n_s/m}\sum_{k=1}^{m} \xi_{kl}\eta_{kl} - \frac{1}{n_s}\left(\sum_{l=1}^{n_s/m}\sum_{k=1}^{m} \xi_{kl}\right)\left(\sum_{l=1}^{n_s/m}\sum_{k=1}^{m} \eta_{kl}\right)\right] \tag{37}$$

If there is a difference of less than 30% between the covariances (or dispersions) determined with equations (36) and (37), then the measurement is considered to be stationary. This is an initial criterion that characterizes the quality of the measurements. For practical use, all data with differences < 30% are of high quality and those with differences between 30% and 60% have an acceptable quality (Foken *et al.*, 1997).

C. Integral Turbulence Test

The integral (normalized) turbulence characteristics (flux variance similarity) may be used together with the non-stationarity test for a check on data quality. This parameter has been investigated extensively by Wichura and Foken (1995).

The integral characteristics of the vertical wind are defined by:

$$\frac{\sigma_w}{u_*} = a_i[\varphi_m(\zeta)]^{b_i} \tag{38}$$

and the integral characteristics of the temperature by:

$$\frac{\sigma_T}{T_*} = a_2[\zeta\varphi_h(\zeta)]^{b_2} \tag{39}$$

where σ_w and σ_T are the vertical velocity and temperature standard deviations, φ_m is the surface layer similarity function, u_* is the friction velocity and ζ is the stability parameter defined as $(h_m - d)/L$, where L is the Obukhov length. The empirical coefficients, a_i and b_i, are obtained with the model of Foken *et al.* (1991) and given in the updated form by Foken *et al.* (1997) in Table 5. According to Foken (1999a) these parameters can also be used for stable stratification. The data quality is good if the difference between the measured integral characteristics and the calculated value differs by not more than 20–30%. For neutral stratification, this test cannot be used for scalar fluxes.

By definition, the integral characteristics are basic similarity characteristics of the atmospheric turbulence (Obukhov, 1960; Wyngaard *et al.*, 1971). Because of the similarity in the basic equations, there is a close connection to the correlation coefficient. Therefore, they characterize whether or not the turbulence is well developed according to the similarity theory of turbulent fluctuations. It is possible to discover some typical effects of non-homogeneous terrain. First, if there is additional mechanical turbulence caused by obstacles or generated by the measuring device itself, the measured values of integral characteristics are significantly higher than predicted by the model. Second, the measured values of integral characteristics are significantly higher than the model for terrain with an inhomogeneity in surface temperature and moisture conditions, but not for inhomogeneities in surface roughness. This was found by De Bruin *et al.* (1991) and confirmed by Wichura and Foken (1995).

D. Energy Balance Closure

A requirement that should be met despite any ecological and climatological differences among the flux study sites is the conservation of energy in the systems, according to the first law of thermodynamics. Thus, the closure of the

Table 5
Coefficients of the normalized turbulence characteristics according to Foken *et al.* (1991, 1997)

	ζ	a_1	b_1	a_2	b_2
σ_w/u_*	$0 > \zeta > -0.032$	1.3	0		
	$-0.032 > \zeta$	2.0	1/8		
σ_u/u_*	$0 > \zeta > -0.032$	2.7	0		
	$-0.032 > \zeta$	4.15	1/8		
σ_T/T_*	$0 > \zeta > -0.0625$			0.5	−1/2
	$-0.0625 > \zeta$			1.0	−1/4

energy balance is a useful parameter to check the plausibility of data sets obtained at different sites. In this approach, the sum of turbulent heat fluxes is compared with the available energy flux (the net radiative flux density less the storage flux densities in the observed ecosystem, including soil, air and biomass). If the energy terms balance each other, the quality of the flux data is considered to be sufficient. However, there are serious objections to this concept, because the radiation fluxes and heat storage terms are also subject to errors. Moreover, under certain meteorological conditions, processes, such as melting, freezing or heat conductance to cold intercepted rain, which are usually not considered in the budget calculation when using a standard set of meteorological observables, may contribute considerably to the energy balance. Under these conditions the closure cannot be taken as a plausibility criterion for flux observations. On the other hand, the apparent lack of energy balance does not constitute conclusive evidence for erroneous turbulent flux measurement, but might indicate the occurrence of other non-vertical and turbulent fluxes (such as advection and subsidence).

Unclosed energy balance has been published for many study sites covering either grasslands or forests, but a comprehensive review of the problem, taking all possible reasons for an unclosed energy balance into account, has still to be carried out (Foken, 1999b). Despite the likely need for a literature review on that particular topic, it is not within the scope of this chapter as it mainly uses the closure of the energy balance as an empirical plausibility criterion for the question of whether or when the vertical turbulent fluxes represent the total fluxes of a scalar.

Ibrom *et al.* (unpublished) developed a statistical procedure to tackle this problem and were able to derive characteristic relationships between the closure of the energy balance and certain meteorological conditions at their study site. These relationships are expected to be influenced by site properties such as fetch, roughness and mesoscale effects. In this investigation, this hypothesis will be tested by comparing the long-term flux data of six EUROFLUX sites.

Table 6 lists the locations and equipment used at the six selected EUROFLUX sites. Although most of the technical details of eddy flux measurements have been harmonized among the EUROFLUX teams, some important aspects of the experimental set-ups, in particular the net radiometer type, were chosen by each group individually. In a field intercomparison of different net radiometers within the Boreal Ecosystem Atmosphere Study (BOREAS) project, Smith *et al.* (1997) observed deviations of up to 16% from their standard device, due mainly to different calibrations of the sensors. The implication is that flux networks such as EUROFLUX need to intercompare the meteorological sensors in addition to the sensors used for flux determination.

To represent the relative degree of energy balance closure (*EBC*) in a data set, the slope of a linear regression, s_1, and the slope of a linear regression

Table 6
Site parameters and sensors used for assessment of energy flux terms at six flux stations

	BE1	FR2	FR1	GE1	GE2	GE3
Location	50° 18′ N 6° 00′ E	44° 42′ N 0° 46′ E	48° 40′ N 7° 05′ E	50° 09′ N 11° 52′ E	50° 58′ N 13° 38′ E	51° 46′ N 9° 35′ E
Elevation	450	60	300	780	380	500
Fetch	300–1500 m	300 to > 1000 m	500 m	200 m	150 to > 500 m	270 to > 500 m
Slope	3%	None	None	None	< 5°	3°
$h_m - d$	11.5 m	12 m	8 m	20 m	20 m	16 m
Net radiation budget	Schenck type 8111	REBS Q7	REBS Q7	Schulze/Däke	Schulze/Däke	Schulze/Däke
Turbulent fluxes	Solent R1024 LI-6262	Solent R1024 LI-6262	Solent R1024 LI-6262	Solent R1024 LI-6262	Solent R1024 LI-6262	USAT-3 LI-6262
High-pass filter	RM (200 s)	RM (200 s)	RM (200 s)	LD	None	LD
Rate of change of heat storage derived from						
Soil	1 profile in 5 depths + humidity profile	4 profiles in 8 depths + humidity profile	Not derived	6 heat flux plates	Heat flux plates	4 profiles in 5 depths
Canopy air space	2 air temperatures in canopy	11 temperatures in canopy	Sonic temperatures at reference height	Temperature and humidity in canopy air	Temperature and humidity in canopy	6 temperatures and humidities in canopy
Biomass	8 temperatures in tree trunks	54 temperatures at different locations	5 × 4 temperatures in tree trunks	Bole temperatures and radiation temperature	Temperature at reference height	1 air temperature

RM, running mean; LD, linear detrend.

forced through the origin, s_2, are used. This is necessary because the linear relationship between turbulent energy fluxes and available energy usually produces a significant intercept. Consequently, *EBC* cannot be represented by one single parameter. The two estimators describe the sensitivity of turbulent heat fluxes to available energy, s_1, and the relative location of the centre of the data with regard to the 1 : 1 line. Under optimal conditions, both should be equal to 1. The data sets are subdivided into classes according to the parameter of interest to investigate the functional relationship between *EBC* and various turbulence parameters (Ibrom *et al.*, unpublished). The calculated *EBC* estimators are then compared with the average value of the parameters given in Table 7.

Figure 6 and Table 7 present individual relationships between the turbulent energy fluxes and the available energy for six EUROFLUX sites. Only data measured at temperatures higher than 1°C were taken into account in order to exclude, for example, the effects of snow and hoarfrost on the measurements. However, rain events that could also have affected the quality of the measurements have not been filtered out from all of the data sets considered here. All data sets have a very similar shape, where a large proportion of the data (60–75%) is located in the region of ± 100 W/m^{-2}. The standard deviation around the regression line is of the same order of magnitude, ranging from 40 to 84 W/m^{-2}. In most cases, the variability of available energy fluxes explains more than 85% of the variance of the fluxes of turbulent energy (Table 7). *EBC* values for whole data sets range from 0.7 to full closure if expressed by the estimator s_1. In all cases, the slope of a linear regression forced to the origin, s_2,

Table 7
Parameters of linear regression of turbulent energy fluxes (i.e. the sum of latent and sensible heat flux against available energy).

Site	Type	Slope	Intercept ($W\,m^{-2}$)	R^2	Root mean square error ($W\,m^{-2}$)
BE1	s_1	0.936	−4.2	0.90	63.0
BE1	s_2	0.926	0.0		63.0
FR2	s_1	0.997	−32.3	0.93	43.6
FR2	s_2	0.892	0.0		49.1
FR1	s_1	0.756	−19.0	0.91	52.8
FR1	s_2	0.713	0.0		54.6
GE1	s_1	0.726	−10.3	0.88	62.4
GE1	s_2	0.704	0.0		62.9
GE2	s_1	0.944	−9.0	0.84	84.1
GE2	s_2	0.922	0.0		84.4
GE3	s_1	0.798	−9.7	0.92	39.4
GE3	s_2	0.773	0.0		40.3

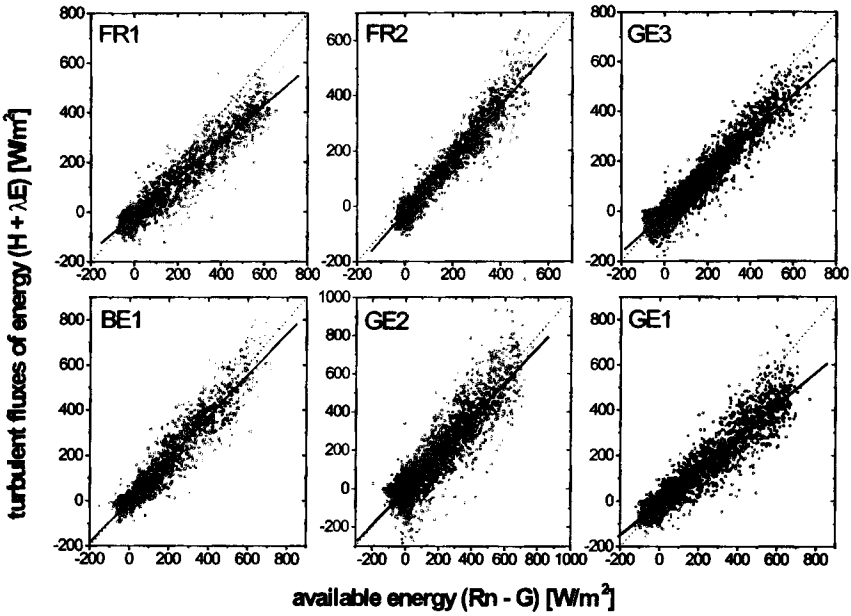

Fig. 6. Scatter diagrams and regression lines of relationship between the turbulent fluxes of energy and available energy fluxes.

is lower than that of the regular regression, s_1, although this effect is not important for the BE1 site. The data set with the highest estimator s_1, FR2, has the lowest negative intercept. Accordingly, the estimator s_2 is about 10% lower than s_1. The estimated relative contribution of the energy storage terms to energy transfer at site FR2 is, on average, twice that for the other sites.

These findings confirm the common observation that the energy balance tends to be more or less unclosed, an indication that non-vertical or non-turbulent fluxes need to be incorporated in the budget calculation, or that there are substantial errors in other energy flux terms which lead to an underestimation of available energy fluxes.

The use of linear regression for the whole data set suppresses the effects of low absolute fluxes. It can be seen at first glance that the relative agreement between turbulently transported energy and available energy is much worse for lower than for higher available energy. Thus it is necessary to go into more detail by using data sets selected by different meteorological conditions. In practice, a relatively large number of parameters could be used to separate the data into subsets and investigate whether they serve as an indicator for the data quality or not, but in most cases the parameters are not independent. The most effective parameters are those connected to

turbulence generation and vertical exchange, such as the normalized stability parameter ζ and friction velocity u_*.

Results of the selective statistical analysis are shown in Figures 7 and 8. All data sets show a common pattern. In conditions of unstable stratification, *EBC* is shown to be high, whereas it is low at stable stratification. The values under neutral stratification are less accurate, because many of the energy flux measurements approach zero and become much smaller than the average standard deviation around the regression line. This effect is shown by the larger standard error of the estimate (bars in Figure 7) and some outliers in the near neutral region. By comparing *EBC* values classified into different stratification regimes with the values for the whole data set (Table 7), it turns out that only the highest *EBC* values at unstable stratification fall in the same range as the high values calculated for the complete data set; already starting with neutral stratification, *EBC* becomes very low at stable stratification.

To complete this brief analysis, *EBC* and friction velocity are compared under two different stratification regimes. Again, the data show a common picture. At both stable and unstable conditions, *EBC* grows with increasing u_* over the whole range at unstable conditions and in the range between zero and 0.4 ms^{-1} at stable stratification. Above the threshold of 0.4 ms^{-1} the estimates

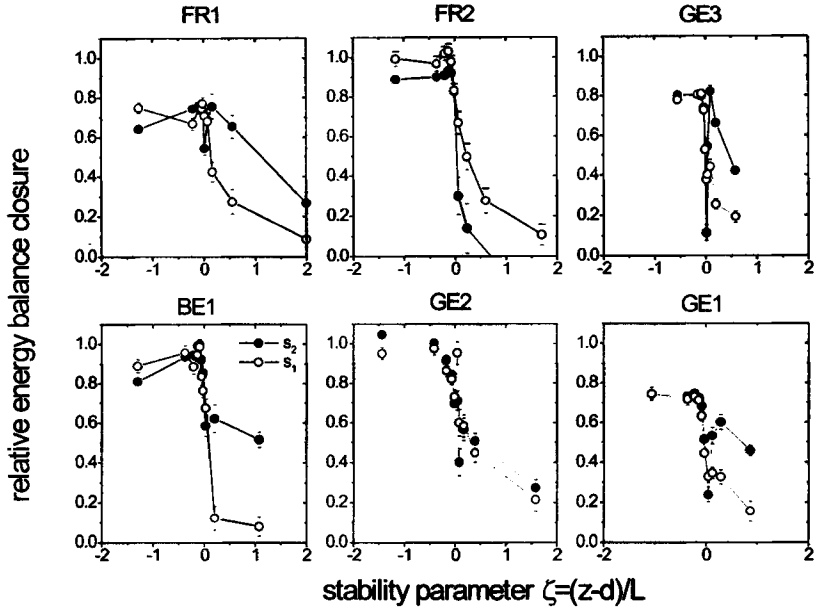

Fig. 7. Functional relationships between the relative energy balance closure and the non-dimensional stability parameter ζ for six EUROFLUX stations.

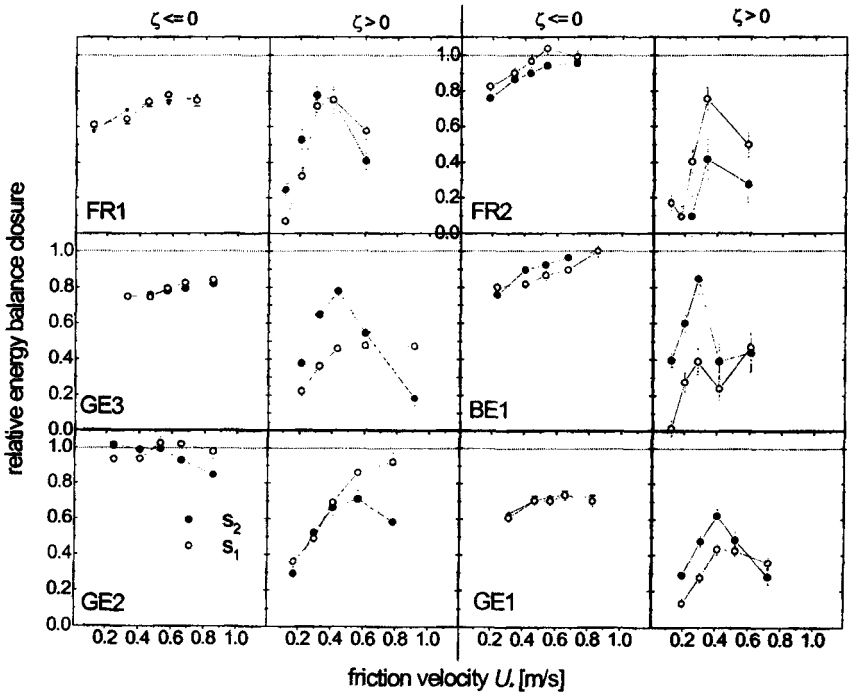

Fig. 8. Functional relationships between the relative energy balance closure and the friction velocity for six EUROFLUX stations.

become less accurate. For near neutral conditions, the energy is very low and small absolute errors become important.

The sensitivity of *EBC* to u_* is much larger at stable than at unstable conditions. This suggests that, at night time, the fluxes could be underestimated owing to a lack of turbulent transport. A similar process is observed for CO_2 fluxes at night (section X). Even if *EBC* appears to be influenced by u_* at stable stratification, this is no evidence for a cause–effect relationship. As expected from its definition, u_* is tightly correlated with the stability parameter ζ. Consequently, classifying the data with u_* will sort the data according to stability as well. Even though distinction cannot be made between different causes, the statistical evidence can be used to derive thresholds of ζ or u_* that are related with a certain degree of *EBC*.

The relationships between *EBC* and turbulence parameters indicate that vertical exchange plays an important role in the distribution of energy fluxes into different non-vertical turbulent fluxes, which are consequently lacking if merely eddy covariance data are used. These effects seem to be general, as they have occurred at all sites investigated. The differences of closure with time, due

to distinct meteorological conditions, seem to be much more important for the quality of flux data than the averaged differences between the sites.

At the moment we are not able to explain the relatively small differences between the sites, because the intercomparison of the net radiometers has not yet been carried out and estimation of the rate of change of energy storage in the biomass and in the soil is still done differently at the different sites. Thus their relative contribution to the energy balance is more likely to be due to different calculation procedures than to real flux differences at the site. These relationships suggest that an even more detailed analysis will prove to be of benefit.

VII. SPATIAL REPRESENTATIVENESS OF MEASURED FLUXES

To cover the widest climate range and as many forest types as possible, the flux measurement network has to consider sites that are not necessarily ideal for eddy covariance measurements. In particular, heterogeneous forests are studied more and more often. The main question for these sites is to know to what extent the fluxes (and the annual sums) are representative of the real ecosystem flux. To know this, it is necessary to locate the flux sources and to establish the distribution of the frequencies at which they influence the flux measurements.

The footprint analysis allows estimation of the source location. It is based on lagrangian analysis and relates the time-averaged vertical flux of a quantity at the measurement point to its turbulent diffusion from sources located upwind from the measurement point. The extent to which an upwind source located a certain distance from the measurement point contributes to observed flux has been termed the source weight function or flux footprint (Schmid, 1994). In footprint analysis, the relationship between the surface sources (downward flux is equivalent to negative sources at the surface) and the measured flux is studied. This can be achieved by analytical (e.g. Schuepp *et al.*, 1990; Horst and Weil, 1994; Schmid, 1994) and stochastic simulation approaches (Leclerc and Thurtell, 1990).

Frequently, the cross-wind integrated footprint models are used to evaluate the adequacy of the fetch of a homogeneous stand in a certain wind direction and under certain stability conditions. This is done by estimating the fraction of flux contributed by the sources within the homogeneous fetch assuming uniform surface sources. Alternatively, an upwind distance giving a significant fraction of flux can be estimated. Different analytical models differ in their complexity. For example, the simplest analytical model by Schuepp *et al.* (1990) for the cross-wind integrated flux footprint, assumes constant wind speed in the vertical and does not explicitly include the effects of atmospheric stability. For the evaluation of cross-wind integrated footprint by a stochastic

approach, a uniquely defined one-dimensional stochastic model (along-wind turbulent dispersion is neglected) for particle trajectories with parameterization for the atmospheric surface layer (Wilson and Sawford, 1996) can be applied.

Table 8 gives estimates of the horizontal position of the footprint peak and the distance for 80% of cumulative footprints by three different footprint models for two measurement height ($h_m - d$) to roughness length (z_0) ratios. The results corresponding to model HW are obtained by applying the approximate version of the analytical model by Horst and Weil (1994), and in stochastic simulations the uniquely defined one-dimensional model was applied. Distances are normalized by height. Of the three models, the HW and stochastic models are in better agreement, while the simplest model by Schuepp *et al.* (1990) predicts further distances for peak location as well as for the 80% cumulative footprint value. The difference is greater for low observation levels relative to roughness length. Of the three models, the more realistic cross-wind integrated footprint models—the Horst and Weil (1994) or the stochastic model—are recommended. Of these, the HW model is easier to apply but, in practice, it cannot be solved for very low measurement height : roughness length ratios.

For measurements above forests, such low values apply (often 20 or even less). Under these conditions, the footprint models designed for application inside the surface layer are not strictly applicable. The stochastic models can be parameterized for more complicated flow conditions and also to account for the roughness sublayer effects above the forest. Baldocchi (1997) has studied the footprint characteristics for the levels inside and above the forest, assuming that the sources are located on the forest floor (in the case of surface-layer footprint analysis, the height of sources is assumed to be $d + z_0$, roughly the upper levels of the canopy, and this level is not permeable for flow). The footprints for measurements inside the forest were observed to be much closer than footprints for measurements inside the surface layer (Baldocchi, 1997). For measurements above the forest, the level of sources is not well defined, but this is not likely to introduce great uncertainty owing to the relatively slow horizontal dispersion inside the canopy.

Table 8
Normalized location of footprint peak ($X_{max}\, h_m^{-1}$) and 80% of cumulative footprint ($X_{80}\, h_m^{-1}$) for three cross-wind integrated footprint models

Model	$X_{max}\, h_m^{-1}$		X80 h_m^{-1}	
	$h_m z_0^{-1} = 20$	$h_m z_0^{-1} = 100$	$h_m z_0^{-1} = 20$	$h_m z_0^{-1} = 100$
Schuepp *et al.* (1990)	6.7	11.4	60.3	102.3
Horst and Weil (1994)	4.2	8.5	44.7	83.5
Wilson and Sawford (1996)*	3.8	9.1	35.4	71.8

*Stochastic simulations with one-dimensional trajectory model.

VIII. SUMMATION PROCEDURE

The net ecosystem exchange is the sum of different physiological components: the gross leaf assimilation, A, and the leaf, wood, root and heterotrophic respiration rates, R_l, R_w, R_r, R_h:

$$N_e = -A + R_l + R_w + R_r + R_h \tag{40}$$

This equation is derived from Ruimy *et al.* (1995) with sign adaptations to fit the meteorological conventions (i.e. positive upwards, negative downwards) According to equation (1), the storage and advection terms are included in N_e. The assimilation and all the respiration terms are positive. The integration of N_e over a given period τ_s gives the net ecosystem production (*NEP*):

$$\mathrm{NEP} = -\int_{t}^{t+\tau_s} N_e \, dt \tag{41}$$

This sum may be directly deduced from eddy covariance and storage flux measurements. The procedure used for the summation, including data gap filling (section IX), night flux corrections (section X) and estimates of uncertainties (section XI), is detailed below.

Other sums of physiological relevance are the net primary productivity (*NPP*) which quantifies the net CO_2 flux exchanged by the vegetation (soil excluded):

$$\mathrm{NPP} = -\int_{t}^{t+\tau_s} (N_e - R_h)\, dt \tag{42}$$

and the gross primary production (GPP) that quantifies the total mass of synthesised glucides:

$$\mathrm{GPP} = -\int_{t}^{t+\tau_s} (N_e - R_l - R_w - R_r - R_h)\, dt \tag{43}$$

However, neither of these can be deduced from flux measurements. The *NPP* calculation requires knowledge of the heterotrophic respiration. This is not available directly even when the eddy covariance system is complemented by soil chambers that measure soil CO_2 fluxes. Indeed, this system does not distinguish between heterotrophic and root respiration.

The *GPP* computation would require the knowledge of the total ecosystem respiration. In particular, it would take into account the difference between day and night-time leaf respiration, which is significant (Ruimy *et al.*, 1995; P.G. Jarvis, personal communication, 1998). This difference cannot be deduced from flux measurements.

Alternative sums may be deduced from the flux measurements as the daytime (night-time) *NEP* is obtained by integration of N_e only on day (night) periods. These quantities do not depend on any data treatment but they cannot be directly related to the fluxes of physiological relevance. A sum currently (but erroneously) named gross primary production (*GPP'*) may currently be deduced using the following procedure:

(1) To liken the night-time CO_2 flux to the total ecosystem respiration ($R_{tot} = R_l + R_w + R_r + R_h$).
(2) To fit a regression equation on the respiration to temperature response.
(3) To use this equation to estimate daytime respiration.
(4) To calculate the summed respiration over day and night.
(5) To deduct this sum from the *NEP*.

Caution is required when calculating this sum to avoid several errors. The night-time fluxes must be selected according to a turbulence criterion in order to eliminate the underestimation error (section X). The temperature used as a reference for the respiration response must be chosen appropriately. To avoid extrapolation errors, it is necessary to choose a temperature for which daytime and night-time ranges are close together. To that end, the soil temperature (i.e. at 2-cm depth) is advisable as a reference as its daily cycle is damped and logged compared to air temperature. It is, of course, a gross simplification to choose a unique reference temperature given that the respiring elements are spread in the ecosystem and are submitted to different temperatures.

Again, in order to minimize the extrapolation error, the regression equation must be chosen so as to provide a non-biased residual distribution. In particular, the modified Arrhénius equation is advisable (Lloyd and Taylor, 1994):

$$R_{tot} = R_{10} \exp\left\{308.56\left(\frac{1}{56.02} - \frac{1}{T_s - 227.13}\right)\right\} \tag{44}$$

whereas the classical exponential regression using R_{10} and Q_{10} parameters is not advisable because it does not reflect correctly the dependence on temperature, Q_{10} being shown to decrease with temperature (Lloyd and Taylor, 1994). The parameterization of R according to temperature could be completed by a response to the soil water content, which is significant on dry soils (FR2). Finally, *GPP'* obtained with the procedure described above differs from *GPP* as it ignores the difference between daytime and night-time leaf respiration.

IX. DATA GAP FILLING

Gaps in long-term data series are almost unavoidable. They may occur as a result of system breaks for routine maintenance or calibration, inadequacy of the meteorological conditions or complete system failures. In EUROFLUX, the effort put into maintenance of the measuring systems reduces the data gaps to less than 15% of the total data. The data gaps may be filled in different ways: interpolation, parameterization or use of a (non-) linear regression equation. By way of example of one approach, gap filling by neural network techniques is described below.

A. Interpolation and Parameterization

The following procedure, using both interpolation and parameterization, may be followed in order to fill the CO_2 flux gaps:

(1) To gather flux data per several day-periods. The length of the period may vary from site to site: it must be short enough for seasonal trends to be insignificant but long enough to allow a reasonable interpolation. For temperate regions, a 10-day period is a good compromise.

(2) For day-time, when Photosynthetic photon flux density (PPFD) is available, to fill data gaps, using a parameterized response of N_e to *PPFD* (exponential, see for example Aubinet *et al.* (unpublished); or hyperbolic, for example Valentini *et al.* (1996). Night-time, when soil temperature is available, to fill data gaps using a parameterized response of N_e to T_s (equation (44)). The parameterization of the N_e to *PPFD* response must be re-evaluated each month to take seasonal fluctuations into account. If necessary, the parameterizations may consider additional variables, such as the air temperature and saturation deficit for day-time data, the soil water content for both day- and night-time data. SVAT models are not recommended for data gap filling when the measured data obtained from this procedure are used for their own calibration and validation. If PPFD or temperature is not available, the data remain missing.

(3) For each half-hour, to sum on the period the corresponding fluxes (measured and parameterized) and to estimate the possible missing data as the corresponding mean.

B. Neural Networks

The data collected at the EUROFLUX stations can be separated into *prognostic* (such as wind speed, temperature, specific humidity, global radiation and incoming long-wave radiation) and *diagnostic* (such as latent heat flux and CO_2 flux) data. For most modelling applications, complete time series of prognostic data are compulsory, whereas diagnostic data are used for calibration and validation of the model only. In that case, complete time series of

the diagnostic data are not needed: short periods with reliable data are generally sufficient. On the other hand, for comparison of diagnostic data between sites, complete time series of those data are a necessity.

As is well accepted by most modellers, the best model to fit a time series is a non-linear regressor (see for example Mihalakakou *et al.*, 1998). The drawback of using it is that there is no information on the system; in other words, it is a complete black box. However, for gap-filling purposes, understanding the underlying physics is not really of interest. For this reason, a non-linear regressor such as a neural network is an excellent tool to fill data gaps. A neural network is especially useful if a full theoretical model cannot be constructed (Gardner and Dorling, 1998). This may be the case if data from other sites are used to fill the gaps, or if relations are described by ill-defined empirical functions, as is the case between global radiation and CO_2 flux. For the examples shown here, the neural network tool of Saxén and Saxén (1995) is used.

1. General Network Architecture

Although it is not possible to prescribe a single configuration of a neural network for all problems, some general considerations can be taken into account. It has been shown (e.g. Huntingford and Cox, 1997) that the architecture of a neural network that will be able to simulate almost any relationship consists of, at least, one hidden layer with four or more nodes. The input nodes have a linear activation function by default; the nodes in the hidden layers should have a logistic or hyperbolic tangent function. The output node may have a linear activation function, which enables the output signal to have any value. It is generally recommended to scale the input signals by using the means and standard deviations of the whole data series. This is to prevent the network from ignoring input nodes with a small range, which may happen if the randomly assigned initial weights are small for the input node with the small range. Also not strictly necessary but recommendable is to remove as much of the expected behaviour of the target variable as possible. This may be done by using as a target value the residue of the original variable minus, for example, the same variable simulated with a simple known physical relation or minus the same variable measured by another instrument. The network can then be used to predict the differences, instead of the actual variable.

Selection of the number of input and hidden nodes is not straightforward. If the number of nodes is too small, the network will fail to converge. On the other hand, too many nodes will result in over-fitting. To decide on the number of hidden nodes, a separate test data set may be fed to the network simultaneously with the training data set. Increasing the number of nodes will increase the degrees of freedom and therefore the goodness-of-fit of the training data set. However, if the goodness-of-fit of the test data set decreases at the same time, this is an indication of over-fitting and the number of nodes should be decreased.

2. *Examples*

As an example, global radiation is simulated. In Figure 9 the network configuration is depicted. As input variables for the network, the air temperature, relative humidity, wind speed and incoming global radiation at the top of the atmosphere are used. The target variable of the network is the residual of the measured global radiation minus a fixed fraction of the global radiation at the top of the atmosphere. The fraction was chosen such that, on a clear day, the residual would be almost zero. As activation function for the input and output nodes, a linear function is used, while for the hidden nodes a sigmoid varying between 0 and 1 is used.

Here the network was used to simulate the effects of clouds on global radiation. The network was trained on a data series of 60 days. Figure 10 shows the results of using the trained network for a separate data set. Although the results are not excellent (on some days the differences may be as large as 200 W m^{-2}), they show that the network is capable of simulating relatively complicated relationships. Possibly the results may be improved by using a longer data set for training and/or other input variables.

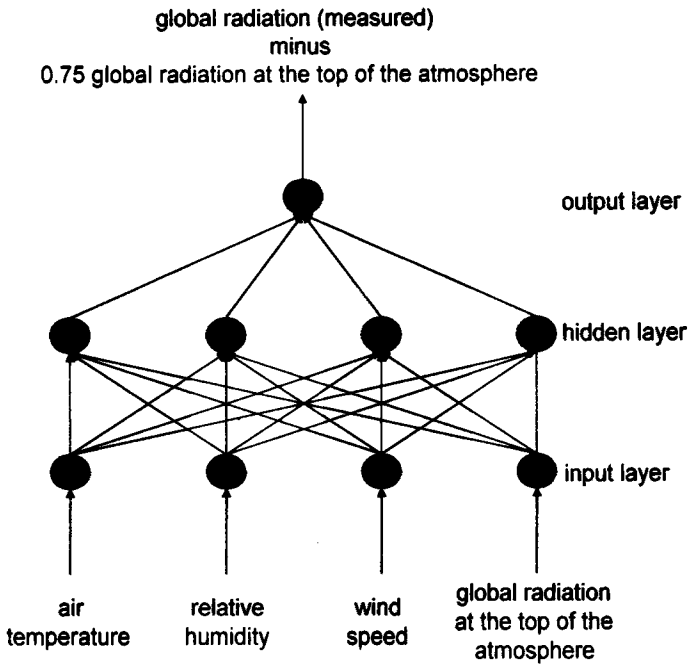

Fig. 9. Example of a neural network configuration with four input signals, one hidden layer with four nodes and one output signal.

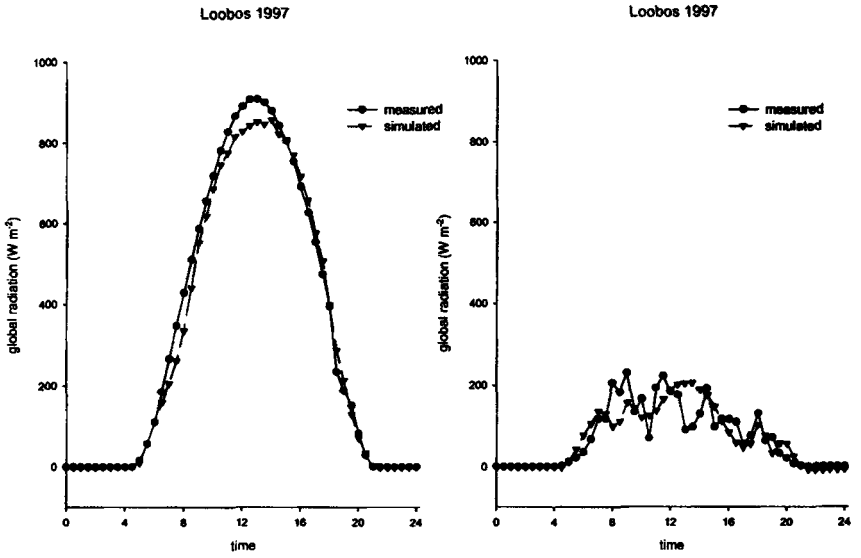

Fig. 10. Simulation of global radiation at a clear day (left) and a cloudy day (right).

In Table 9 the regression results are presented for the training and validation data sets. Here the regression results are also shown filling gaps in data series of the latent heat flux and the CO_2 flux. For the latent heat flux, the target variable was the residual between the measured flux and the flux calculated using the Penman–Monteith equation with a fixed surface resistance of 100 s m^{-1} for dry conditions and of zero for wet conditions. The global radiation, temperature, humidity deficit, soil moisture content at 50 cm depth and precipitation rate were used as driving variables to explain

Table 9
Results of the regression of simulated versus measured data

Variable	Constant	Slope	R^2
Global radiation (c)	25.60 W m^{-2}	0.85	0.85
Global radiation (v)	33.68 W m^{-2}	0.89	0.79
Latent heat flux (c)	7.95 W m^{-2}	0.78	0.68
Latent heat flux (v)	40.61 W m^{-2}	0.60	0.55
Carbon flux (c)	−1.04 μmol m^{-2} s^{-1}	0.79	0.75
Carbon flux (v)	−0.15 μmol m^{-2} s^{-1}	0.90	0.69
Carbon flux as a function of global radiation	−4.47 μmol m^{-2} s^{-1}	0.36	0.44

The (c) indicates calibration results, while (v) stands for validation results.

the residual. One month of data was used for calibration and another month for validation. This period is probably too short. Huntingford and Cox (1997) used a neural network to simulate the stomatal conductance and found that the neural network could explain 74% of the variance in their test data set. The carbon flux was simulated using a neural network and an empirical relationship. The neural network used global radiation, air temperature, net radiation, soil temperature, soil moisture content, CO_2 concentration in the trunk space, sensible heat flux, latent heat flux and friction velocity as input variables, with carbon flux as the target variable. To train the network, 40 days of 30-min data were used. For validation, an extra 10-day period was used. Only daytime values were considered. For the training period, the network explained 75% of the variance, while for the validation data set this decreased to 69%. To compare this with a conventional method of filling data gaps, a non-linear relationship between carbon flux and global radiation was used. The performance of such a relation is much worse in comparison with the network results (see Table 9).

These results show the benefits of using a neural network, especially if there is no need to investigate the physical relations of the processes, as when the prime purpose is to fill gaps in data series. It should be borne in mind that a neural network is suitable only to interpolate. Extrapolation outside the range of the training data may lead to unexpected results. More suggestions on the use of a neural network for atmospheric sciences are given by Gardner and Dorling (1998).

X. CORRECTIONS TO NIGHT-TIME DATA

There is some likelihood that, during stable night-time conditions, CO_2 exchange is underestimated by the eddy covariance measurements. This is supported by the apparent correlation between u_* (used as a measure for turbulent mixing) and CO_2 efflux during the night (Grace *et al.*, 1996; Goulden *et al.*, 1996a). Indeed, night-time efflux resulting from ecosystem respiration is controlled mainly by temperature and soil water content; it should be independent of turbulence if correlations between u_* and temperature are removed. Turbulence may, however, affect soil respiration by 'pressure pumping' at high levels of u_*, but in the range of interest for stable night-time conditions there is no evidence for that. Moreover, the relation between $\overline{EBC}$ and u_* observed under stable conditions at different sites (Figure 8) confirms that the observed underestimation of the CO_2 fluxes at night comes from a lack of turbulence rather than a varying CO_2 source strength. Underestimation of the night-time CO_2 flux is an example of a selective systematic error and as such can be a serious problem, particularly when long-term budgets are estimated by integration of short-term flux measurements (Moncrieff *et al.*, 1996).

Stable nights increase the importance of accounting for storage of CO_2 in the layer below the eddy flux system. CO_2 stored within the forest during the night can be partly assimilated in the morning and partly flushed out. Although this leads to a discrepancy between released CO_2 and measured flux in the short term, it does not affect the long-term budget as long as the morning flush is captured by the measurement. It would appear that storage may not account for the total loss of fluxes, and some of the CO_2 that is released by the soil and the vegetation seems to leave the forest by as yet unquantified routes. Possible mechanisms may be katabatic flow or high-frequency fluctuations that are not detected (Goulden *et al.*, 1996a; Moncrieff *et al.*, 1996), slow diffusion or local convection cells. There is some evidence that some CO_2 does leave the forest vertically, without being measured by the eddy covariance system, when storage of CO_2 above the eddy correlation system exceeds the measured flux (Figure 11).

A way to correct for flux underestimation during stable nights is to replace the measured fluxes by the simulated efflux estimated by a temperature function derived during well-mixed conditions. Two general problems with

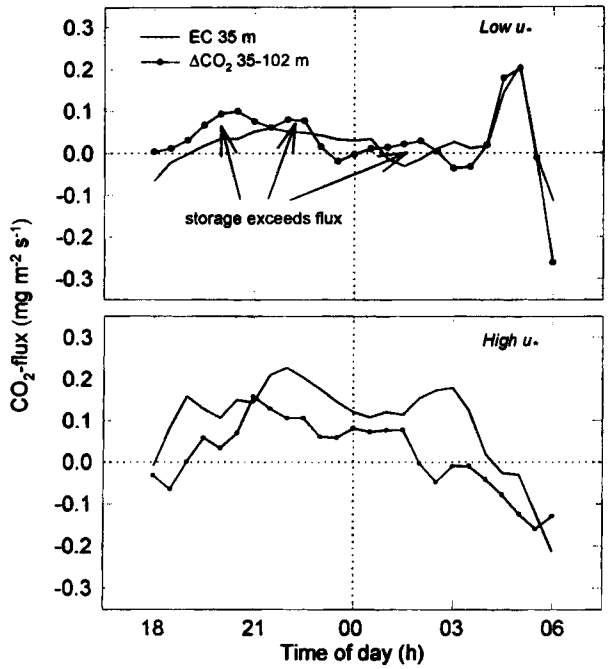

Fig. 11. CO_2 flux measured by eddy correlation and CO_2 storage above the eddy correlation system during a calm and a well-mixed night at Norunda, central Sweden.

this approach are: (1) the sensitivity of the CO_2 budget to the threshold value of u_* that is used to distinguish between stable and well-mixed conditions (Grelle, 1997); and (2) the potential risk of 'double counting' if there is a morning flush of CO_2.

To estimate the effects of night-time stability on night-time fluxes at various sites, nocturnal CO_2 release was plotted against friction velocity for ten EUROFLUX sites (Figure 12). To reduce the scatter, data have been sorted by u_* in intervals of 0.05 m s^{-1}. To eliminate correlations between u_* and temperature, the CO_2 fluxes have been normalized with the simulated flux estimated by a temperature function. For some sites, however, a representative temperature function could not be established with the available data, either because variations in temperature were too small or because there were too few occasions with well-mixed conditions. In these instances, data were confined to a narrow temperature range (1.5 K) and normalized by the 'saturation value' reached at high friction velocities. These two approaches have also been used by Goulden *et al.* (1996a).

The results for the different EUROFLUX sites are shown in Figure 12. By weighting the relative underestimations with the frequency distribution of the friction velocity, a relative loss of CO_2 efflux can be estimated (Figure 13). Because of the different normalizing procedures used for individual sites, the saturation value of the normalized efflux was taken as the reference for zero loss rather than the 1.0 constant.

This is a rather rough estimation which generally depends on the time period and the number of data points. However, it gives a clue to the importance of storage for the correction of short-term night-time fluxes at the individual sites.

XI. ERROR ESTIMATION

Many of the potential sources of error have been described in preceding sections, for example errors introduced by non-steady-state conditions, advection, complex terrain and instrumentation error. Every flux network operates within the constraints imposed upon it by natural variability in atmospheric and surface properties. Wesely and Hart (1985) estimated that such variability, in combination with instrumentation errors, restricts the accuracy of an individual turbulent flux measurement to between 10% and 20%. If the errors are random, then integrating the individual half-hourly flux estimates over a day will improve this figure, and thus daily integrals are likely to be reasonable. Businger (1986) investigated errors between different eddy covariance systems and found that, in general, systematic errors of the order of 30% or more, and random errors of the same magnitude, existed. The network approach, of course, removes some of this potential source of error by harmonizing the instrumentation and software across sites. At any one site, a careful review of all the components in an eddy covariance system is essential. In one

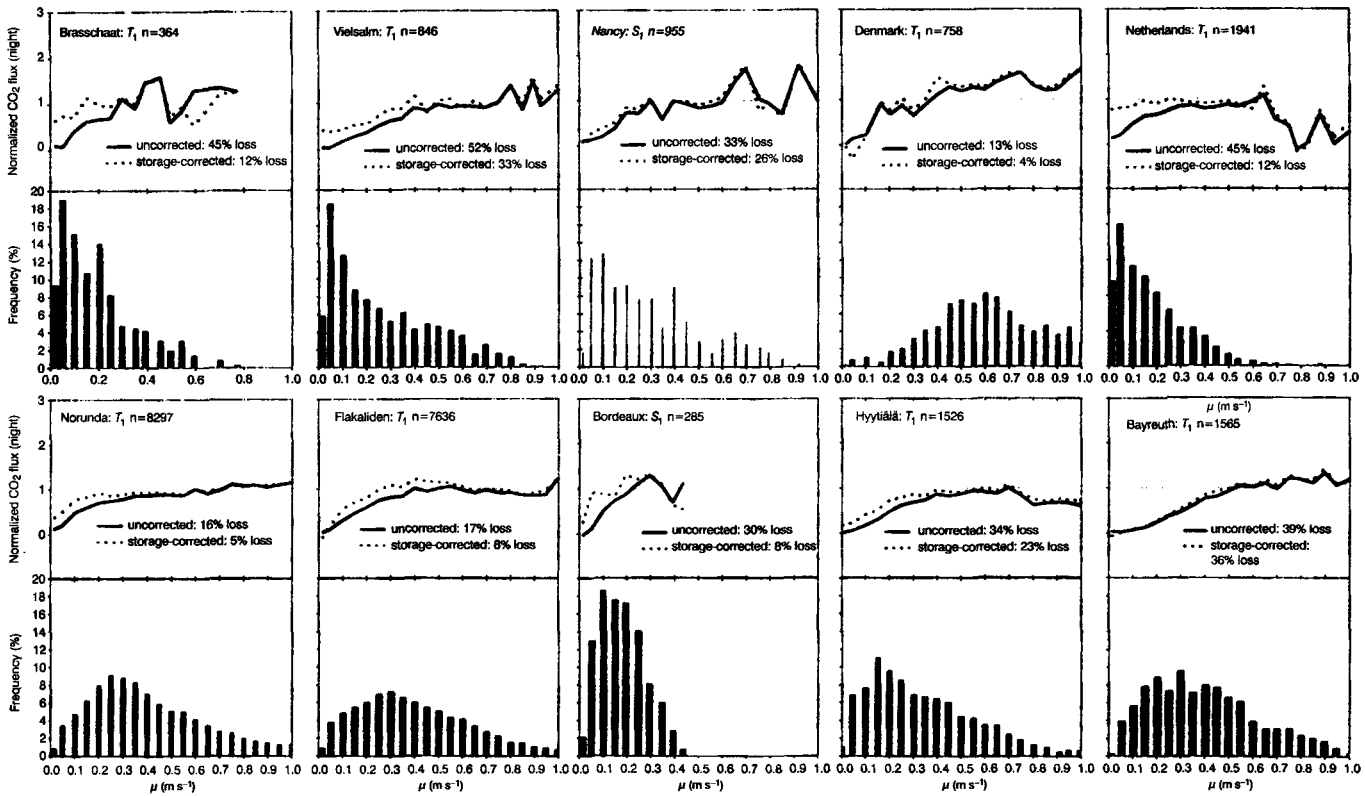

Fig. 12. Normalized night-time CO_2 fluxes at 10 EUROFLUX sites sorted by friction velocity into intervals of 0.05 m s^{-1}. Normalization is done either by a temperature response function (T) or by the saturation value (S). n = number of data points.

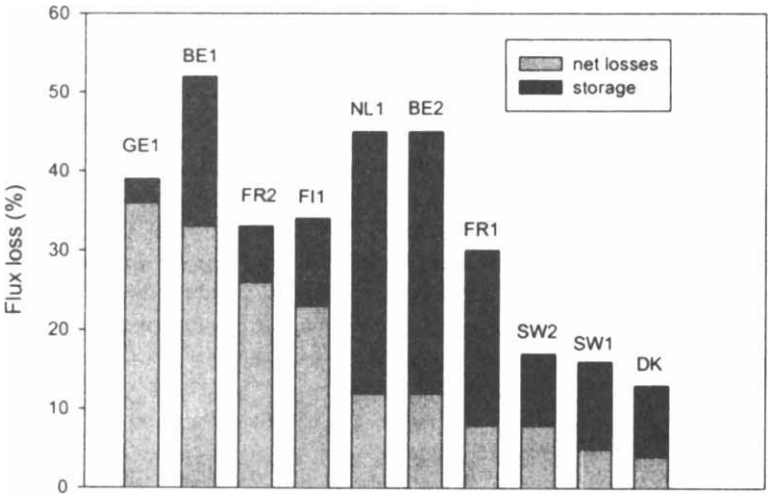

Fig. 13. Relative loss of night-time fluxes for 10 EUROFLUX sites and the storage component.

of the few papers describing errors in long-term flux studies, Goulden *et al.* (1996a) suggested that the long-term precision of their eddy covariance flux measurements was ± 5%, and they estimated that their annual net canopy exchange of carbon should be regarded as being within ± 30 g C m^{-2} $year^{-1}$.

The EUROFLUX partners have adopted the error terminology defined by Moncrieff *et al.* (1996), i.e. that errors can loosely be either random and/or systematic (the latter being subdivided into full or selective errors) and that a full error analysis is essential for published flux estimates. In addition, flux estimates from EUROFLUX will be published as $X \pm a \pm b$, where X is the mean value of the result, a is the estimate of stochastic (random) uncertainty, and b is an assessment of systematic uncertainty because of possible systematic errors in the system. Many of the quality checks applied within EUROFLUX as part of the accepted methodology will isolate gross errors and inconsistencies, and careful calibration and analysis routines will help to prevent the more insidious selective systematic errors. Errors will remain, however, and must continually be checked for and eliminated.

One method that is useful for predicting the likely impact on integral flux estimates of different types of error follows the procedure outlined in Moncrieff *et al.* (1996). In brief, it is desirable to produce daily plots of CO_2 and H_2O fluxes averaged over a particular time period, such as a week or a month, and then to apply 'errors' of different types and magnitudes to those mean values at different times of the day or night. The advantage of this approach is that it permits the unequivocal nature of the source or sink of

carbon, for instance, to be stated with some justification. The net flux over the mean daily cycle is directly proportional to the overall net flux over the measurement period. This approach is valid as long as the basic character of the daily cycle does not vary significantly from day to day.

XII. CONCLUSIONS

To meet the requirement for information about biosphere–atmosphere interactions, several measurement networks have been originated. The EUROFLUX network, aiming at measuring long-term net carbon dioxide and water vapour exchanges between European forests and the atmosphere, was first initiated in 1996. It was followed in 1998 by the Ameriflux (northern and central America) and Medeflu (Mediterranean countries) networks, as well as the tentative global NETFLUX network, which pursue the same goals. Further networks in Japan, Australasia and southern America are planned. At present, in 1998, about 80 stations measuring CO_2 and H_2O fluxes exchanged by different ecosystems with the atmosphere are to be found around the world; the number is growing and there is a call for the stations to constitute a permanent network operating like surface weather station networks (Running *et al.*, unpublished).

The history of surface weather stations teaches us that an essential requirement for such a task is the standardization of the measurement procedure. In the present case, the eddy covariance method was chosen on all sites because it is the only method that allows direct measurement of the fluxes at the ecosystem scale (several hectares), at a half-hourly time-scale and continuously over several years. However, standardization of the eddy covariance method requires not only the choice of a common measurement system, but also the setting up of a procedure for computing, correcting, summing and checking the quality of the measurements.

In EUROFLUX, standardization of the measurement system was achieved from the beginning, as each team agreed to use the same system. It comprises a three-dimensional sonic anemometer coupled with a closed-path infrared gas analyser. Reliability, handling facilities but also commercial availability of the system motivated this choice. In addition to this, a standard measurement procedure had to be achieved. The aim of this chapter was to present this.

Computation of the fluxes from instantaneous measurements is a complex procedure (to give an idea, one half-hourly flux derives from more than 22 400 instantaneous measurements) that includes high-pass filtering, time-lag estimation, mean and (co)-variance computation, co-ordinate rotation, and conversion from covariances to fluxes. In this chapter we have proposed a standard way of achieving these operations and have presented a method for testing the software that performs them.

The fluxes are also subject to full or selective systematic errors due to instrument limitations or non-ideal meteorological conditions. Thus, a correction must be introduced. We have compared different approaches for correcting the fluxes and, finally, have proposed a standard method. In addition, we have proposed a series of tests for assessing the quality of the measurements as well as different methods that allow prediction of the spatial representativeness of the fluxes.

Half-hourly fluxes must be summed in order to give the annual net exchanges of CO_2 and H_2O. We have discussed the relevancy of different variables and have presented procedures for data gap filling. Finally, we described a way of estimating the error.

All the procedures described in this chapter represent the present state-of-the-art in EUROFLUX. They are followed by the 12 teams of the group. We propose them as a standard procedure to be used by all eddy covariance measuring stations.

ACKNOWLEDGEMENTS

This research was supported by European Commission, Programme Environment and Climate 1994–1998, Project EUROFLUX under contract ENV4-CT95-0078. This work is the result of many people's efforts. The authors acknowledge all the scientists as well as all the technicians who, thanks to their continuous work, made the realization of this paper possible (with apologies to people who have been forgotten here): Jean-Marc Bonnefond, Reinhart Ceulemans, Lars Christensen, Michael Courtney, Han Dolman, Patrick Gross, John Hansen, Paul Jarvis, Poul Hummelshoej, Niels-Otto Jensen, Petri Keronen, Fred Kockelbergh, Tapio Lahti, Anders Lindroth, Giorgio Matteucci, Eddy Moors, Toivo Pohja, S.L. Scott, Erkki Siivola, John Tenhunen and Michel Yernaux.

REFERENCES

Aubinet, M., Chermanne, B., Vandenhaute, M., Longdoz, B., Yernaux, M. and Laitat, E. (unpublished). Long term measurements of water vapour and carbon dioxide fluxes above a mixed forest in Ardenne's region.

Baldocchi, D. (1997). Flux footprints within and over forest canopies. *Boundary-Layer Meteorol.* **85**, 273–292.

Baldocchi, D. and Meyers, T.D. (1991). Trace gas exchange above the floor of a deciduous forest. 1. Evaporation and CO_2 efflux. (1991) *J. Geophys. Res.* **96**(D4), 7271–7285.

Baldocchi, D., Hicks., B.B. and Meyers, T.D. (1988). Measuring biosphere–atmosphere exchanges of biologically related gases with micrometeorological methods. *Ecology* **69**, 1331–1340.

Baldocchi, D., Valentini, R., Oechel, W. and Dahlman, R. (1996). Strategies for measuring and modelling carbon dioxide and water vapour fluxes over terrestrial ecosystems. *Global Change Biol.* **2**, 159–168.

Baldocchi, D., Vogel, C.A. and Hall, B. (1997). Seasonal variation of carbon dioxide exchange rates above and below a boreal jack pine forest. *Agric. For. Metereol.* **83**, 135–146.

Baldocchi, D., Wilson, K. and Paw, U.K.T. (unpublished). On measuring net ecosystem carbon exchange in complex terrain over tall vegetation.

Black, T.A., Den Hartog, G., Neumann, H.H., Blanken, P.D., Yang, P.C., Russell, C., Nesic, Z., Lee, X., Chen, S.G., Staebler R. and Novak, M.D. (1996). Annual cycles of water vapour and carbon dioxide fluxes in and above a boreal aspen forest. *Global Change Biol.* **2**, 219–229.

De Bruin, H.A.R., Bink, N.J. and Kroon, L.J.M. (1991). Fluxes in the surface layer under advective conditions. In: *Workshop on Land Surface Evaporation Measurement and Parametrization* (Ed. by T.J. Schmugge and J.C. André), pp. 157–169. Springer, New York.

Businger, J.A. (1986). Evaluation of the accuracy with which dry deposition can be measured with current micrometeorological techniques. *J. Clim. Appl. Meteorol.* **25**, 1100–1124.

Desjardins, R.L. (1985). Carbon dioxide budget of maize. *Agric. For. Meteorol.* **36**, 29–41.

Foken, Th. (1999a). The turbulence experiment FINTUREX at the Neumayer-Station/Antartica. *Ber. des Deutschen Wetterdienstes,* Berlin (in press).

Foken, Th. (1999b). Die scheinbar ungeschlossene Energiebilanz am Erdboden-, eine Herausforderung an die Experimentelle Meteorologie. *Sitzungsberichte der Leibnitz-Sozietaet,* Berlin (in press).

Foken, Th. and Wichura, B. (1996). Tools for quality assessment of surface-based flux measurements. *Agric. For. Meteorol.* **78**, 83–105.

Foken, Th., Skeib, G. and Richter, S.H. (1991). Dependence of the integral turbulence characteristics on the stability of stratification and their use for Doppler–Sodar measurements. *Z. Meteorol.* **41**, 311–315.

Foken, Th., Jegede, O.O., Weisensee, U., Richter, S.H., Handorf, D., Görsdorf, U., Vogel, G., Schubert, U., Kirzel, H.-J. and Thiermann, V. (1997). Results of the LINEX-96/2 experiment. *Deutscher Wetterdienst, Geschäftsbereich Forschung und Entwicklung, Arbeitsergebnisse* **48**, 75 pp.

Gardner, M.W. and Dorling, S.R. (1998). Artificial neural networks (the multilayer perception)—a review of applications in the atmospheric sciences. *Atmos. Environ.* **32**, 2627–2636.

Gash, J.H.C. and Culf, A.D. (1996). Applying linear detrend to eddy correlation data in real time. *Boundary-Layer Meteorol.* **79**, 301–306.

Goulden, M.L., Munger, J.W., Fan, S.-M., Daube, B.C. and Wofsy, S.C. (1996a). Measurements of carbon sequestration by long-term eddy covariance: methods and a critical evaluation of accuracy. *Global Change Biol.* **2**, 159–168.

Goulden, M.L., Munger, J.W., Fan, S.-M., Daube, B.C. and Wofsy, S.C. (1996b). Exchange of carbon dioxide by a deciduous forest: response to interannual climate variability. *Science* **271**, 1576–1578.

Grace, J., Malhi, Y., Lloyd, J., McIntyre, J., Miranda, A.C., Meir, P. and Miranda, H.S. (1996). The use of eddy covariance to infer the net carbon dioxide uptake of Brazilian rain forest. *Global Change Biol.* **2**, 209–217.

Greco, S. and Baldocchi, D. (1996). Seasonal variations of CO_2 and water vapour exchange rates over a temperate deciduous forest. *Global Change Biol.* **2**, 183–197.

Grelle, A. (1996). *SOLCOM: Gill Solent Communication software.* Technical note. Department for production ecology. Faculty of forestry. Swedish University of Agricultural Sciences, Uppsalla.

Grelle, A. (1997). *Long-term Water and Carbon Dioxide Fluxes from a Boreal Forest: Methods and Applications.* PhD thesis. Swedish University of agricultural studies, Uppsalla.

Grelle, A. and Lindroth, A. (1994). Flow distortion by a solent sonic anemometer: wind tunnel calibration and its assessment for flux measurements over forest and field. *J. Atmos. Oceanic Technol.* **11**, 1529–1542.

Grelle, A. and Lindroth, A. (1996). Eddy-correlation system for long term monitoring of fluxes of heat, water vapour, and CO_2. *Global Change Biol.* **2**, 297–307.

Grelle, A., Lohse, H. and Peters, G. (1994). Central ice station. In: *The Expedition ARKTIS-IX/1 of RV "Polarstern" in 1993. Berichte zur Polarforschung* 134.

Gurjanov, A.A., Zubkovskii, S.L. and Fedorov, M.M. (1984). Mnogoknal'naja avtomatizirov-annaja sistema obrabotki signalov no baze EVM. *Geod. Geophys. Veröff.* **RII**(26), 17–20.

Haataja, J. and Vesala, T. (1997). *SMEAR II, Station for Measuring Forest Ecosystem–Atmosphere Relation.* University of Helsinki, Department of Forest Ecology Publications, Helsinki, Finland.

Højstrup, J. (1993). A statistical data screening procedure. *Meas. Sci. Technol.* **48**, 472–492.

Hollinger, D.Y., Kelliher, F.M., Byers, J.N., Hunt, J.E., McSeveny, T.M. and Weir, P.L. (1994). Carbon dioxide exchange between an undisturbed old-growth temperate forest and the atmosphere. *Ecology* **75**(1), 134–150.

Horst, T.W. (1997). A simple formula for attenuation of eddy fluxes measured with first order response scalar sensors. *Boundary-Layer Meteorol.* **82**, 219–233.

Horst, T.W. and Weil, J.C. (1994). How far is far enough? The fetch requirements for micrometeorological measurement of surface fluxes. *J. Atmos. Oceanic Technol.* **11**, 1018–1025.

Houghton, J.J., Meiro Filho, L.G., Callander, B.A., Harris, N., Kattenberg, A. and Maskell, K. (1996). *Climate Change 1995: The Science of Climate Change.* Cambridge University Press, Cambridge.

Houghton, R.A., Davidson, E.A. and Woodwell, G.M. (1998). Missing sinks, feedbacks, and understanding the role of terrestrial ecosystems in the global carbon balance. *Global Biogeochem. Cycles* **12**, 25–34.

Huntingford, C. and Cox, P.M. (1997). Use of statistical and neural network techniques to detect how stomatal conductance responds to changes in the local environment. *Ecol. Model.* **80**, 217–246.

Ibrom, A., Morgenstern, K., Richter, I., Falk, M., Oltchev, A., Constantin, J. and Gravenhorst, G. (unpublished). The energy balance: implications for the quality assessment of eddy covariance measurements above a forest canopy.

Jarvis, P.G., Massheeder, J.M., Hale, S.E., Moncrieff, J.B., Rayment, M. and Scott, S.L. (1997). Seasonal variation of carbon dioxide, water vapor, and energy exchanges of a boreal black spruce forest. *J. Geophys. Res.* **102**(D24), 28953–28966.

Kaimal, J.C. and Finnigan, J.J. (1994). *Atmospheric Boundary Layer Flows: Their Structure and Measurement.* Oxford University Press, Oxford.

Kaimal, J.C. and Gaynor, J.E. (1991). Another look at sonic thermometry. *Boundary-Layer Meteorol.* **56**, 401–410.

Kaimal, J.C., Wyngaard, J.C., Izumi, Y. and Cote, O.R. (1972). Spectral characteristics of surface-layer turbulence. *Q.J.R. Meteorol. Soc.* **98**, 563–589.

Kristensen, L. (1998). *Time Series Analysis. Dealing with Imperfect Data.* Risø National Laboratory, Roskilde, Denmark.

Leclerc, M.Y. and Thurtell, G.W. (1990). Footprint prediction of scalar fluxes using a Markovian analysis. *Boundary-Layer Meteorol.* **52**, 247–258.

Lee, X. (1998). On micrometeorological observations of surface–air exchange over tall vegetation. *Agric. For. Meteorol.* **91**, 39–49.

Lenshow, D.H. and Raupach, M.R. (1991). The attenuation of fluctuations in scalar concentrations through sampling tubes. *J. Geophys. Res.* **96**, 5259–5268.

Leuning, R. and Judd, M.J. (1996). The relative merits of open- and closed-path analysers for measurements of eddy fluxes. *Global Change Biol.* **2**, 241–254.

Leuning, R. and King, K.M. (1992). Comparison of eddy-covariance measurements of CO_2 fluxes by open-and-closed-path CO_2 analysers. *Boundary-Layer Meteorol.* **59**, 297–311.

Leuning, R. and Moncrieff, J. (1990). Eddy-covariance CO_2 measurements using open- and closed-path CO_2 analysers: corrections for analyser water vapor sensitivity and damping of fluctuations in air sampling tubes. *Boundary-Layer Meteorol.* **53**, 63–76.

LI-COR (1991) *LI-6262 CO_2 H_2O Analyser Instruction Manual.* LI-COR, Lincoln, Nebraska.

Lindroth, A., Grelle, A. and Moren, A.-S. (1998). Long-term measurements of boreal forest carbon balance reveal large temperature sensitivity. *Global Change Biol.* **4**, 443–450.

Lloyd, C.R., Shuttleworth, W.J., Gash, J.H.C. and Turner, M. (1984). A microprocessor system for eddy-correlation. *Agric. For. Meteorol.* **33**, 67–80.

Lloyd, J. and Taylor, J.A. (1994). On the temperature dependence of soil respiration. *Funct. Ecol.* **8**, 315–323.

McMillen, R.T. (1986). *A BASIC Program for Eddy Correlation in Non Simple Terrain.* NOAA Technical Memorandum, ERL ART-147. NOAA, Silver Spring, Maryland.

McMillen, R.T. (1988). An eddy correlation technique with extended applicability to non-simple terrain. *Boundary-Layer Meteorol.* **43**, 231–245.

Mahrt, L. (1991). Eddy asymmetry in the sheared heated boundary layer. *J. Atmos. Sci.* **4**, 153–157.

Martin, P.H., Valentini, R., Jacques, M., Fabbri, K., Galati, D., Quaratino, R. *et al.* (1998). A new estimate of the carbon sink strength of EU forests integrating flux measurements, field surveys, and space observations: 0.17–0.35 Gt(C). *Ambio* **27**, 582–584.

Massman, W.J. (1991). The attenuation of concentration fluctuations in turbulent-flow through a tube. *J. Geophys. Res.* **96**, 5269–5273.

Mihalakakou, G., Santamouris, M. and Asimakopoulos, D. (1998). Modelling ambient air temperature time series using neural networks. *J. Geophys. Res.* **103**, 19509–19517.

Moncrieff, J.B., Mahli, Y. and Leuning, R. (1996). The propagation of errors in long-term measurements of land–atmosphere fluxes of carbon and water. *Global Change Biol.* **2**, 231–240.

Moncrieff, J.B., Massheder, J.M., de Bruin, H., Elbers, J., Friborg, T., Heusinkveld, B., Kabat, P., Scott, S., Soegaard, H. and Verhoef, A. (1997a). A system to measure surface fluxes of momentum, sensible heat, water vapour and carbon dioxide. *J. Hydrol.* **188–189**, 589–611.

Moncrieff, J.B., Valentini, R., Greco, S., Seufert, G. and Ciccioli, P. (1997b). Trace gas exchange over terrestrial ecosystems: methods and perspectives in micrometeorology. *J. Exp. Bot.* **48**, 1133–1142.

Monin, A.S. and Yaglom, A.M. (1971). *Statistical Fluid Mechanics, Mechanics of Turbulence.* MIT Press, Cambridge, Massachusetts.

Moore, C.J. (1986). Frequency response corrections for eddy correlation systems. *Boundary-Layer Meteorol.* **37**, 17–35.

Obukhov, A.M. (1960). O strukture temperaturnogo polja i polja skorostej v uslovijach konvekcii. *Izv. AN SSSR. ser. geofiz.* 1392–1396.

Peters, G., Claussen, M., Lohse, H., Grelle, A., Kornblüh, L. and Fischer, B. (1993). Ice floe station. In: *ARKTIS 1993. Ber. Nr. 11 Ber. aus dem ZMK. A: Meteorology.* Hamburg University, Department of Meteorology, Hamburg.

Rannik, Ü. and Vesala, T. (1999). Autoregressive filtering versus linear detrending in estimation of fluxes by the eddy covariance method. *Boundary-Layer Meteorol.* **91**, 259–280.

Rannik, Ü., Vesala, T. and Keskinen, R. (1997). On the damping of temperature fluctuations in a circular tube relevant to the eddy covariance measurement technique. *J. Geophys. Res.* **102**, 12789–12794.

Ruimy, A., Jarvis, P.G., Baldocchi, D. and Saugier, B. (1995). CO_2 fluxes over plant canopies and solar radiation: a review. *Adv. Ecol. Res.* **26**, 1–69.

Running, S.W., Baldocchi, D., Cohen, W., Gower, S.T., Turner, D., Bakwin, P. and Hibbard, K. (unpublished). A global terrestrial monitoring network scaling tower fluxes with ecosystem modeling and EOS satellite data.

Saigusa, N., Oikawa, T. and Liu, S. (1998). Seasonal variations of the exchanges of CO_2 and H_2O between a grassland and the atmosphere: an experimental study. *Agric. For. Meteorol.* **89**, 131–139.

Saxén, B. and Saxén, H. (1995). *NNDT—A Neural Network Development Tool. Version 1.2.* Åbo Akademi University, Åbo, Finland.

Schimel, S.D. (1995). Terrestrial ecosystems and the global carbon cycle. *Global Change Biol.* **1**, 77–91.

Schmid, H.P. (1994). Source areas for scalars and scalar fluxes. *Boundary-Layer Meteorol.* **67**, 293–318.

Schotanus, P., Nieuwstadt, F.T.M. and de Bruin, H.A.R. (1983). Temperature measurement with a sonic anemometer and its application to heat and moisture flux. *Boundary-Layer Meteorol.* **26**, 81–93.

Schuepp, P.H., Leclerc, M.Y., MacPherson, J.I. and Desjardins, R.L. (1990). Footprint prediction of scalar fluxes from analytical solutions of the diffusion equation. *Boundary-Layer Meteorol.* **50**, 355–373.

Shuttleworth, W.J. (1988). Corrections for the effect of background concentration change and sensor drift in real-time eddy correlation systems. *Boundary-Layer Meteorol.* **42**, 167–180.

Smith, E.A., Hodges, G.B., Bacrania, M., Cooper, H.J., Owens, M.A., Chappell, R. and Kincannon, W. (1997). *BOREAS Net Radiometer Engineering Study: Final Report.* Grant NAG5-4447. NASA.

Stull, R.B. (1988). *An Introduction to Boundary Layer Meteorology.* Kluwer Academic, Dordrecht.

Swinbank, W.C. (1951). The measurement of vertical transfer of heat and water vapour by eddies in the lower atmosphere. *J. Meteorol.* **8**, 135–145.

Valentini, R., Scarascia Mugnozza, G.E., De Angelis, P. and Bimbi, R. (1991). An experimental test of the eddy correlation technique over a Mediterranean macchia canopy. *Plant Cell Environ.* **14**, 987–994.

Valentini, R., De Angelis, P., Matteucci, G., Monaco, S., Dore, S. and Scarascia Mugnozza, G.E. (1996). Seasonal net carbon dioxide exchange of a beech forest with the atmosphere. *Global Change Biol.* **2**, 199–207.

Verma, S.B., Baldocchi, D.D., Anderson, D.E., Matt, D.R. and Clement, R.J. (1986). Eddy fluxes of CO_2, water vapor and sensible heat over a deciduous forest. *Boundary-Layer Meteorol.* **36**, 71–91.

Verma, S.B., Kim, J. and Clement, R. (1989). Carbon dioxide, water vapor and sensible heat fluxes over a tallgrass prairie. *Boundary-Layer Meteorol.* **46**, 53–67.

Vermetten, A.W.M., Ganzenveld, L., Jeuken, A., Hofschreuder, P. and Mohren, G.M.J. (1994). CO_2 uptake by a stand of Douglas fir: flux measurements compared with model calculation. *Agric. For. Meteorol.* **72**, 57–80.

Vickers, D. and Mahrt, L. (1997). Quality control and flux sampling problems for tower and aircraft data. *J. Atmos. Oceanic Technol.* **14**, 512–526.

Webb, E.K., Pearman, G.I. and Leuning, R. (1980). Correction of flux measurements for density effects due to heat and water vapour transfer. *Q. J. R. Meteorol. Soc.* **106**, 85–100.

Wesely, M.L. and Hart, R.L. (1985). Variability of short term eddy-correlation estimates of mass exchange. In: *The Forest–Atmosphere Interaction* (Ed. by B.A. Hutchison and B.B. Hicks), pp. 591–612. D. Reidel, Dordrecht.

Wichura, B. and Foken. Th. (1995). *Anwendung integraler Turbulenzcharakteristiken zur Bestimmung von Beimengungen in der Bodenschicht der Atmosphäre.* DWD, Abteilung Forschung, Arbeitsergebnisse, No. 29 Deutscher wetterdierst, Offenbuch.

Wilson, J.D. and Sawford, B.L. (1996). Review of lagrangian stochastic models for trajectories in the turbulent atmosphere. *Boundary-Layer Meteorol.* **78**, 191–210.

Wofsy, S.C., Goulden, M.L., Munger, J.W., Fan, S.-M., Bakwin, P.S., Daube, B.C., Bassow, S.L. and Bazzaz, F.A. (1993). Net exchange of CO_2 in a mid-latitude forest. *Science* **260**, 1314–1317.

Wyngaard, J.C., Coté, O.R. and Izumi, Y. (1971). Local free convection, similarity and the budgets of shear stress and heat flux. *J. Atmos. Sci.* **28**, 1171–1182.

APPENDIX A

Computation of the Two-axis Rotation Matrix Elements

Two rotations are successively applied around the z and y axes. The first aligns u into the x direction in the x–z plane and nullifies v, according to:

$$u_{1,i} = \sum_j A_{01,ij} \cdot u_{0,j} \tag{A1a}$$

with

$$A_{01} = \begin{pmatrix} \cos\theta & \sin\theta & 0 \\ -\sin\theta & \cos\theta & 0 \\ 0 & 0 & 1 \end{pmatrix} \tag{A1b}$$

and where the rotation angle, its cosine and sine are:

$$\theta = \tan^{-1}\left(\frac{\bar{v}_0}{\bar{u}_0}\right), \quad \cos\theta = \frac{\bar{u}_0}{\sqrt{\bar{u}_0^2 + \bar{v}_0^2}}, \quad \sin\theta = \frac{\bar{v}_0}{\sqrt{\bar{u}_0^2 + \bar{v}_0^2}} \tag{A1c}$$

The second rotation forces u to point along the mean wind direction. It nullifies w according to:

$$u_{2,j} = \sum_j A_{12,i,j} \cdot u_{i,j} \tag{A2a}$$

with

$$A_{12} = \begin{pmatrix} \cos\phi & 0 & \sin\phi \\ 0 & 1 & 0 \\ -\sin\phi & 0 & \cos\phi \end{pmatrix} \tag{A2b}$$

and where the rotation angle is:

$$\phi = \tan^{-1}\left(\frac{\overline{w}_1}{\overline{u}_1}\right) \tag{A2c}$$

That is, in terms of the non-rotated components of the velocity:

$$\phi = \tan^{-1}\left(\frac{\overline{w}_0}{\sqrt{\overline{u}_0^2 + \overline{v}_0^2}}\right), \cos\phi = \frac{\sqrt{\overline{u}_0^2 + \overline{v}_0^2}}{\sqrt{\overline{u}_0^2 + \overline{v}_0^2 + \overline{w}_0^2}}, \sin\phi = \frac{\overline{w}_0}{\sqrt{\overline{u}_0^2 + \overline{v}_0^2 + \overline{w}_0^2}} \tag{A2d}$$

The two-rotation matrix is obtained by multiplication of the single rotation matrices:

$$A_{02} = A_{12} \cdot A_{01} \tag{A3}$$

Finally, by introducing in equation (A3) the expressions (A1b) and (A2b) of the single-axis rotation matrix, in which the sine and cosine functions are expressed according to (A1c) and (A2d), we obtain:

$$A_{02} = \begin{pmatrix} \dfrac{\overline{u}_0}{\sqrt{\overline{u}_0^2 + \overline{v}_0^2 + \overline{w}_0^2}} & \dfrac{\overline{v}_0}{\sqrt{\overline{u}_0^2 + \overline{v}_0^2 + \overline{w}_0^2}} & \dfrac{\overline{w}_0}{\sqrt{\overline{u}_0^2 + \overline{v}_0^2 + \overline{w}_0^2}} \\ -\dfrac{\overline{v}_0}{\sqrt{\overline{u}_0^2 + \overline{v}_0^2}} & \dfrac{\overline{u}_0}{\sqrt{\overline{u}_0^2 + \overline{v}_0^2}} & 0 \\ -\dfrac{\overline{u}_0\overline{w}_0}{\sqrt{\overline{u}_0^2 + \overline{v}_0^2 + \overline{w}_0^2}\sqrt{\overline{u}_0^2 + \overline{v}_0^2}} & -\dfrac{\overline{v}_0\overline{w}_0}{\sqrt{\overline{u}_0^2 + \overline{v}_0^2 + \overline{w}_0^2}\sqrt{\overline{u}_0^2 + \overline{v}_0^2}} & \dfrac{\sqrt{\overline{u}_0^2 + \overline{\mu}_0^2}}{\sqrt{\overline{u}_0^2 + \overline{v}_0^2 + \overline{w}_0^2}} \end{pmatrix} \tag{A4}$$

APPENDIX B

Computation of the Third Axis Rotation

The third rotation is performed around the x axis:

$$\begin{pmatrix} u_3 \\ v_3 \\ w_3 \end{pmatrix} = \begin{pmatrix} 1 & 0 & 0 \\ 0 & \cos\psi & \sin\psi \\ 0 & -\sin\psi & \cos\psi \end{pmatrix} \cdot \begin{pmatrix} u_2 \\ v_2 \\ w_2 \end{pmatrix} \tag{B1}$$

and nullifies the $v'w'$ covariances. Kaimal and Finnigan (1994) showed that the angle that fulfilled this condition is:

$$\psi = \frac{1}{2}\tan^{-1}(2Y), \text{ with } Y = \frac{\overline{v}_2\overline{w}_2}{\overline{v}_2^2 - \overline{w}_2^2} = \frac{\overline{v}_2'\overline{w}_2'}{\overline{v}_2'^2 - \overline{w}_2'^2} \tag{B2}$$

Consequently, the sine and cosine functions are:

$$\cos\psi = \left(\frac{1+\left(1+4Y^2\right)^{-1/2}}{2}\right)^{1/2}, \quad \sin\psi = \left(\frac{1-\left(1+4Y^2\right)^{-1/2}}{2}\right)^{1/2} \tag{B3}$$

and the matrix A_{23}:

$$A_{23} = \begin{pmatrix} 1 & 0 & 0 \\ 0 & \left(\dfrac{1+\left(1+4Y^2\right)^{-1/2}}{2}\right)^{1/2} & \left(\dfrac{1-\left(1+4Y^2\right)^{-1/2}}{2}\right)^{1/2} \\ 0 & -\left(\dfrac{1-\left(1+4Y^2\right)^{-1/2}}{2}\right)^{1/2} & \left(\dfrac{1+\left(1+4Y^2\right)^{-1/2}}{2}\right)^{1/2} \end{pmatrix} \tag{B4}$$